Theory of Sputtering. I. Sputtering Yield of Amorphous and Polycrystalline Targets*

PETER SIGMUND†
Metallurgy Division, Argonne National Laboratory, Argonne, Illinois 60439
(Received 3 April 1969)

Sputtering of a target by energetic ions or recoil atoms is assumed to result from cascades of atomic collisions. The sputtering yield is calculated under the assumption of random slowing down in an infinite medium. An integrodifferential equation for the yield is developed from the general Boltzmann transport equation. Input quantities are the cross sections for ion-target and target-target collisions, and atomic binding energies. Solutions of the integral equation are given that are asymptotically exact in the limit of high ion energy as compared to atomic binding energies. Two main stages of the collision cascade have to be distinguished: first, the slowing down of the primary ion and all recoiling atoms that have comparable energies—these particles determine the spatial extent of the cascade; second, the creation and slowing down of low-energy recoils that constitute the major part of all atoms set in motion. The separation between the two stages is essentially complete in the limit of high ion energy, as far as the calculation of the sputtering yield is concerned. High-energy collisions are characterized by Thomas-Fermi-type cross sections, while a Born-Mayer-type cross section is applied in the low-energy region. Electronic stopping is included when necessary. The separation of the cascade into two distinct stages has the consequence that two characteristic depths are important for the qualitative understanding of the sputtering process. First, the scattering events that eventually lead to sputtering take place within a certain layer near the surface, the thickness of which depends on ion mass and energy and on ion-target geometry. In the elastic collision region, this thickness is a sizable fraction of the ion range. Second, the majority of sputtered particles originate from a very thin surface layer ($\sim$5 Å), because small energies dominate. The general sputtering-yield formula is applied to specific situations that are of interest for comparison with experiment. These include backsputtering of thick targets by ion beams at perpendicular and oblique incidence and ion energies above $\sim$100 eV, transmission sputtering of thin foils, sputtering by recoil atoms from α-active atoms distributed homogeneously or inhomogeneously in a thick target, sputtering of fissionable specimens by fission fragments, and sputtering of specimens that are irradiated in the core of a reactor or bombarded with a neutron beam. There is good agreement with experimental results on polycrystalline targets within the estimated accuracy of the data and the input parameters entering the theory. There is no need for adjustable parameters in the usual sense, but specific experimental setups are discussed that allow independent checks or accurate determination of some input quantities.

1. INTRODUCTION

In recent years, a large number of experimental results on sputtering by energetic particle bombardment has been accumulated. Most experiments dealt with measurements of the sputtering yield versus energy for many ion-target combinations, but a significant amount of work also has been done in investigating the angular and energy distribution of sputtered particles, or their average energy. In many experimental setups the angle of incidence could be varied, and among other parameters of interest were target temperature and ion dose. Sputtering experiments have been done on amorphous targets, polycrystals of various degrees of texture, and single crystals. Also the geometry of the experiments has differed widely. Although bombardment of plane target surfaces and observation of "backward sputtering" has been most frequent in recent years, other possibilities were quite common: sputtering of wires and balls, transmission sputtering of thin foils, sputtering by recoil atoms from sources embedded in thick targets, and, recently, sputtering by fast neutrons. Although considerable discrepancies still exist in the experimental results produced by various groups, some standards have developed concerning the basic requirements for reproducible and reliable experiments. This development is clearly reflected in recent reviews of Behrisch,[1] Kaminsky,[2] Carter and Colligon,[3] and Pleshivtsev.[4]

Theoretical efforts have been increasingly successful in the last fifteen years in understanding the main features of sputtering in terms of a series of quasi-elastic collision processes induced by the bombarding ion. Usually the first collision does not lead to backward sputtering directly; at least for perpendicular incidence a hit target atom always has a velocity component in the direction away from the target surface (Fig. 1). Thus, sputtering is a typical multiple collision process involving a cascade of moving target atoms. This cascade may extend over a considerable region inside the target, but for sputtering, only the intersection with one or more of the target surfaces is of interest.

While the concept of a collision cascade governing the sputtering process is a common feature in all recent sputtering theories, there are considerable differences

* Work was performed under the auspices of the U. S. Atomic Energy Commission.
† Visiting Scientist on leave from Kernforschungsanlage, Jülich, Germany.

[1] R. Behrisch, Ergeb. Exactk. Naturw. **35**, 295 (1964).
[2] M. Kaminsky, *Atomic and Ionic Impact Phenomena on Metal Surfaces* (Springer-Verlag, Berlin, 1965).
[3] G. Carter and J. S. Colligon, *Ion Bombardment of Solids* (Elsevier Publishing Co., Inc., New York, 1968).
[4] N. V. Pleshivtsev, *Cathode Sputtering* (in Russian) (Atomizdat, Moscow, 1968).

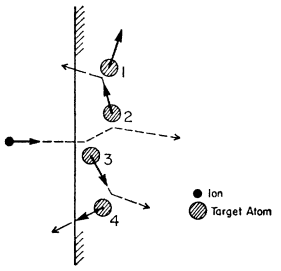

FIG. 1. Series of collision processes leading to sputtering of atoms 2 and 4.

in the basic processes that various authors consider responsible for sputtering. In a number of theories it has been assumed that the majority of atoms are sputtered by random collision processes, even in crystals.[5–12] Other authors assumed that regular lattice structure causes other than random collision processes to dominate sputtering of both single and polycrystals.[13–15] There have been discussions on the role of focused collision chains in the ejection process[14–18] and the role of channeling and transparency in the anisotropy of the sputtering yield of single crystals.[14,15,18,19] Another discussion on where the sputtered particles come from in the random ejection theories has been carried on less explicitly. In Refs. 6, 8, 11, 12, and 16, mostly surface atoms account for the sputtering yield, whereas in Refs. 5, 7, and 10, a great deal of the sputtered atoms must have travelled some distance through the crystal before being ejected.

The arguments used in the above discussions are based mainly on experimental results, and secondly on evidence from computer simulation. The "pure" theorist had little information available on collision cascades that was based on calculations from first principles and accurate enough to stand an argument. Because of the complexity of the problem, it was necessary in all theories quoted above either to introduce a number of extra assumptions that ought to be *results* of a theory (if valid at all) or to introduce a number of adjustable parameters that determine the radius of a cascade, the number of atoms set in motion, the surface binding energy, etc. An additional uncertainty pertinent to the earlier treatments[5–9] was a lack of knowledge of interatomic potentials and collision cross sections that has been removed at least partially later.

It is the purpose of this and two following papers to present a systematic theory of sputtering on the basis of a minimum of assumptions. Necessary basic assumptions concern the characteristics of a *single* collision (differential cross section, inelastic stopping), the structure of the medium (random or crystalline), the structure and binding forces of the surface, and some factors that depend on specific experimental arrangements like beam-target geometry, high or low ion energy, etc.

A useful starting point for this program is the sputtering of a *random target*, since collision cascades in random media are governed by the equations of transport theory, and a good deal of experience has been collected recently on application of these equations to slowing down of ions. Lindhard *et al.*[20] established cross sections governing collisions of ions and atoms in the keV region from Thomas-Fermi theory and showed that one can predict ion ranges accurately by using these cross sections.[21] Sanders[22] generalized Lindhard's procedure to calculate the spatial extension of a collision cascade and the momentum distribution of recoiling atoms. Sanders based his treatment on the power approximation of the Thomas-Fermi scattering cross section[20] and the assumption that all collisions are elastic. This is a specific case where many calculations can be performed by exact methods.[21–25] The power cross sections are accurate enough to allow comparison with experimental results over limited ranges of ion energy.[21,24,25]

A very successful calculation of an *emission* problem on the basis of transport theory was performed by Hachenberg and Brauer,[26] who treated electron-electron emission. The present theory is somewhat similar to

[5] F. Keywell, Phys. Rev. **97**, 1611 (1955).
[6] D. E. Harrison, Phys. Rev. **102**, 1473 (1956); **105**, 1202 (1957); J. Chem. Phys. **32**, 1336 (1960).
[7] D. T. Goldman and A. Simon, Phys. Rev. **111**, 383 (1958); R. S. Pease, in *Proceedings of the International School of Physics "Enrico Fermi" Course* (Academic Press Inc., New York, 1964), Vol. 13, p. 158; Yu. V. Bulgakov, Zh. Tekhn. Fiz. **33**, 500 (1963) [English transl.: Soviet Phys.—Tech. Phys. **8**, 369 (1963)].
[8] E. Langberg, Phys. Rev. **111**, 91 (1958).
[9] P. K. Rol, J. M. Fluit, and J. Kistemaker, Physica **26**, 1009 (1960).
[10] W. Brandt and R. Laubert, Nucl. Instr. Methods **47**, 201 (1967).
[11] P. Joyes, J. Phys. (Paris) **29**, 774 (1968).
[12] M. W. Thompson, Phil. Mag. **18**, 377 (1968).
[13] M. W. Thompson, in *Proceedings of the Fifth International Conference on Ionization Phenomena in Gases, Munich, 1961* (North-Holland Publishing Co., Amsterdam, 1962), p. 85; the model proposed in this paper has been improved and extended by many authors since 1962.
[14] D. E. Harrison, N. S. Levy, J. P. Johnson, and H. M. Effron, J. Appl. Phys. **39**, 3742 (1968); Appl. Phys. Letters **8**, 33 (1966).
[15] D. Onderdelinden, Can. J. Phys. **46**, 739 (1968); thesis, University of Leiden, 1968 (unpublished); this thesis contains a list of references on the "transparency model."
[16] C. Lehmann and P. Sigmund, Phys. Status Solidi **16**, 507 (1966).
[17] N. T. Olson and H. P. Smith, Phys. Rev. **157**, 241 (1967); R. G. Musket and H. P. Smith, J. Appl. Phys. **39**, 3579 (1968); T. B. Higgins, N. T. Olson, and H. P. Smith, *ibid.* **39**, 4849 (1968).
[18] S. A. Drentje, thesis, University of Groningen, 1968 (unpublished).
[19] D. Onderdelinden, Appl. Phys. Letters **8**, 189 (1966).
[20] J. Lindhard, V. Nielsen, and M. Scharff, Kgl. Danske Videnskab. Selskab, Mat.-Fys. Medd. **36**, No. 10 (1968).
[21] J. Lindhard, M. Scharff, and H. E. Schiøtt, Kgl. Danske Videnskab. Selskab, Mat.-Fys. Medd. **33**, No. 14 (1963).
[22] J. B. Sanders, thesis, University of Leiden, 1968 (unpublished).
[23] M. T. Robinson, Phil. Mag. **12**, 741 (1965); **17**, 639 (1968).
[24] P. Sigmund and J. B. Sanders, in *Proceedings of the International Conference on "Application of Ion Beams to Semiconductor Technology,"* edited by P. Glotin (Editions Ophrys, Paris, 1967), p. 215.
[25] J. B. Sanders, Can. J. Phys. **46**, 455 (1968).
[26] O. Hachenberg and W. Brauer, Advan. Electron. Electron Phys. **11**, 413 (1959).

theirs. The only pervious attempt to base a *sputtering* theory on Boltzmann's equation is Harrison's.[6] Joyes[11] made a compromise by applying transport theory to one part of the sputtering process and single collision arguments to another. The methods of transport theory in general have been discussed most extensively in monographs on neutron transport theory (e.g., Ref. 27).

A qualitative picture of the sputtering of a random target by an ion beam looks as follows. An impinging ion undergoes a series of collisions in the target, and atoms that recoil with sufficient energy undergo secondary collisions, thereby creating another generation of recoiling atoms. Both the ion itself and energetic recoil atoms have the possibility of getting scattered back through the surface by a series of collisions from a depth that may be a certain fraction of the total ion range. These back-scattered ions and energetic recoil atoms account for most of the sputtered *energy*[28,29] but constitute only a minor portion of the number of sputtered *atoms*. Note that the energy distribution of sputtered atoms peaks heavily at very small energies.[12] The slowing-down paths of both the ion and all energetic recoils are surrounded by clouds of higher-order recoil atoms with very low energy. These atoms have small ranges and therefore can only get sputtered if they are located originally within a couple of atomic layers from the surface. But there are so many of them that they account for the major portion of the sputtering yield.

A yield calculation consists of a number of steps: (1) to determine the amount of energy deposited by energetic particles (ion and recoil atoms) near the surface; (2) to convert this energy into a number of low-energy recoil atoms; (3) to determine how many of these atoms come to the very surface; and (4) to select those atoms that have sufficient energy to overcome the surface binding forces. These steps will be visible in the mathematical treatment, although there will be needed only one basic equation to determine the sputtering yield, and not four. Also, the order in which the above steps enter the theory will deviate from the chronological order. The essential input quantities are the cross sections for scattering of high-energy ions and atoms [steps (1) and (2)], the cross section for scattering of low-energy atoms [steps (2) and (3)], and the surface binding forces [step (4)]. While good high-energy cross sections are avialable,[20] we have to allow for some uncertainty with respect to the latter two quantities. It will turn out that they determine first of all the absolute magnitude of the sputtering yield, while the variation of the yield with the atomic number of the ion, ion energy, and angle of ion incidence is insensitive to these quantities, at least at ion energies that are large compared to the threshold energy for sputtering (~20 eV). Only such ion energies will be considered in this paper, since the surface collisions that dominate sputtering near threshold cannot be described by transport theory.

It is the opinion of the author that the mechanism sketched above accounts for the main features of sputtering of amorphous and liquid targets, and that only some modifications have to be applied in order to describe the dominant effects of the regular lattice structure in single-crystal sputtering. The anisotropy of the *sputtering yield* is accounted for by a reduction of the energy deposited near the surface when bombardment is along a channeling direction.[15,18,19] Provided that there is a "compensation" of this orientation effect,[30] random slowing down of the *ion* can be assumed when the sputtering yield of a *polycrystal* is calculated.[19] The anisotropy of the *ejection pattern* is consistent with the assumption that those collisions that lead to actual ejection of an atom are governed by the regular surface structure.[16] There may be a contribution of focused collision chains to the sputtering yield that will not average out in case of a polycrystal. If this contribution were substantial, the sputtering yield of a polycrystal would be greater than that of an otherwise identical amorphous target. It has been pointed out[16] that the contribution is small, first of all since no appreciable temperature dependence of the experimental sputtering yields of polycrystals[31,32] has been found. Single-crystal yields[32] are inconclusive, since the temperature dependence found there is sensitively anisotropic, and thus dominated by the ion, rather than the ejection characteristics. An important point is the observation that in single crystals sputtered by heavy ions at various energies preferred ejection only accounts for a minor portion of the sputtering yield.[17,33] Theoretical considerations of two groups of authors[16,34] gave roughly identical results, but led to opposite conclusions, since Lehmann and the present author assumed that the maximum focuson range is of the order of 10 interatomic distances or less at room temperature, while Nelson and Jan assumed considerably longer ranges. There is no reliable experimental information available on focuson ranges. Computer simulation suggested only a small contribution of focusons[14,35] to sputtering. Most of Harrison's[14] results, however, were produced under conditions where focusons are not expected to be significant.

In the present paper we make use of the working

[27] B. Davidson, *Neutron Transport Theory* (Clarendon Press, Oxford, 1957).
[28] P. Sigmund, Can. J. Phys. **46**, 731 (1968).
[29] H. H. Andersen, Appl. Phys. Letters **13**, 85 (1968).
[30] J. Lindhard, Kgl. Danske Videnskab. Selskab, Mat.-Fys. Medd. **34**, No. 14 (1965).
[31] R. S. Nelson, Phil. Mag. **11**, 291 (1965).
[32] I. N. Evdokimov, V. A. Molchanov, D. D. Odintsov, and V. M. Chicherov, Dokl. Akad. Nauk SSSR **177**, 550 (1967) [English transl.: Soviet Phys.—Doklady **12**, 1050 (1968)].
[33] F. Schulz and R. Sizmann, (to be published); F. Schulz, thesis, University of Munich, 1967 (unpublished).
[34] R. S. Nelson and R. V. Jan, Can. J. Phys. **46**, 747 (1968).
[35] R. N. Schlaug, thesis, University of California, Berkeley, 1965 (unpublished).

hypothesis that the sputtering yield of a polycrystal can be calculated by assuming random slowing down throughout the cascade. Otherwise there would only be very few experimental sputtering yields of amorphous oxides and liquids to compare with. The effect of focusons will be included in a later paper, together with a more detailed discussion of single-crystal sputtering. It should be stressed that a consistent theory for a random target is an important and probably necessary first step toward an understanding of sputtering of crystalline targets, irrespective of the significance of lattice effects.

In the present paper the emphasis is on sputtering *yields* under various bombardment conditions, i.e., ion beams over a large energy range at perpendicular or oblique incidence, backward and transmission sputtering, sputtering by radioactive or fission sources, and neutron sputtering. Energy distributions and ejection characteristics will be treated in a subsequent paper (II).

The basic transport equation that governs the sputtering of a random target with a plane surface will be derived in Sec. 2. The equation contains eight variables, but it is reduced to an equation for the sputtering yield for several geometries in Sec. 3, whereby five variables can be eliminated. In the same section, the equation is reduced further to a set of integral equations with only one variable by taking spatial moments and expanding the angular dependence in terms of Legendre polynomials. In Sec. 4 the input quantities are discussed, and analytic solutions of the moment equations are presented. A general sputtering-yield formula is derived, and its implications are discussed. Section 5 deals with applications. The case of homogeneous isotropic source is simplest and is discussed in Sec. 5 A. In all other cases it is necessary to reconstruct spatial distribution functions from moments. The general procedure and application to transmission sputtering and other possible experiments are discussed in Sec. 5 B. Backward sputtering of thick and thin targets is considered in Sec. 5 C.

2. BASIC EQUATIONS

For convenience we assume a target with a planar surface. The results of the theory can be applied directly to other targets like wires, etc., since the radius of a wire is usually large compared to the dimensions of a collision cascade. Microscopic deviations from a planar surface will be discussed later.

Let us assume an atom starting its motion at a time $t=0$ in a plane $x=0$ (Fig. 2), with an arbitrary velocity vector $\mathbf{v}$. The basic quantity of interest is the function

$$G(x,\mathbf{v}_0,\mathbf{v},t)d^3v_0dx\,, \tag{1}$$

which is the average number of atoms moving at time t in a layer (x,dx) with velocity $(\mathbf{v}_0,d^3v_0)$. The number of atoms with velocity $(\mathbf{v}_0,d^3v_0)$ penetrating the plane

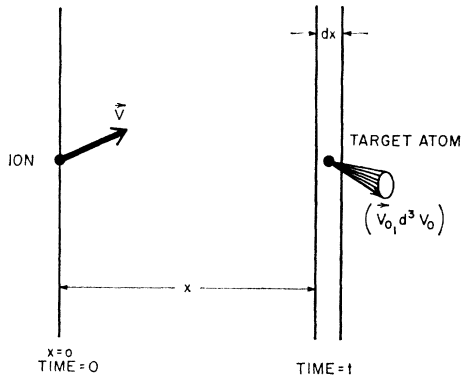

FIG. 2. Geometry of sputtering calculation.

x in a time interval dt is given by

$$G(x,\mathbf{v}_0,\mathbf{v},t)d^3v_0|v_{0x}|dt\,, \tag{2}$$

where v_{0x} is the x component of $\mathbf{v}_0$,

The sputtering yield for backward sputtering of a target with a plane surface at $x=0$ is then

$$S=\int d^3v_0|v_{0x}|\int_0^\infty dt\,G(0,\mathbf{v}_0,\mathbf{v},t)\,, \tag{3}$$

where the integration over d^3v_0 extends over all $\mathbf{v}_0$ with *negative* x components large enough to overcome surface binding forces. Similarly, the yield of transmission sputtering through a surface at $x=d$ is given by

$$S=\int d^3v_0v_{0x}\int_0^\infty dt\,G(d,\mathbf{v}_0,\mathbf{v},t)\,, \tag{4}$$

where v_{0x} must be *positive*.

In an isotropic and homogeneous medium, the function $G(x,\mathbf{v}_0,\mathbf{v},t)$ will satisfy Boltzmann's equation

$$\frac{1}{v}\frac{\partial}{\partial t}G(x,\mathbf{v}_0,\mathbf{v},t)-\eta\frac{\partial}{\partial x}G(x,\mathbf{v}_0,\mathbf{v},t)=N\int d\sigma[G(x,\mathbf{v}_0,\mathbf{v},t)-G(x,\mathbf{v}_0,\mathbf{v}',t)-G(x,\mathbf{v}_0,\mathbf{v}'',t)]\,, \tag{5a}$$

where (Fig. 3) v is the $|\mathbf{v}|$, N is the density of target atoms, $d\sigma$ is the differential cross section $[=d\sigma(\mathbf{v},\mathbf{v}',\mathbf{v}'')=K(\mathbf{v},\mathbf{v}',\mathbf{v}'')d^3v'd^3v'']$, $\mathbf{v}'$ is the velocity of scattered particle, $\mathbf{v}''$ is the velocity of recoiling atom, and η is the v_x/v.

Equation (5a) differs from the usual form[27] in that we deal with a "forward equation," where $\mathbf{v}$ is the variable and $\mathbf{v}_0$ a parameter, while the reverse is true for the "backward" form used in neutron transport theory. Another important difference is that we deal with two "scattering" terms instead of only one, since the effect of the recoiling atom has been taken into account in the last term on the right-hand side.

Equation (5) is derived by a standard argument (see,

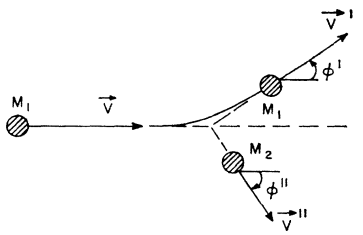

FIG. 3. Geometry of a single-scattering event: laboratory system.

for example, Refs. 21 and 22). Consider a particle moving at $t=0$ in $x=0$. After a time δt, it may or may not have made a collision. Hence,

$$G(x,\mathbf{v},\mathbf{v}_0,t)=N v\delta t\int d\sigma[G(x,\mathbf{v}_0,\mathbf{v}',t)+G(x,\mathbf{v}_0,\mathbf{v}'',t)]$$
$$+\left(1-N v\delta t\int d\sigma\right)G(x-\eta v\delta t,\ \mathbf{v}_0,\ \mathbf{v},\ t-\delta t).$$

The first term on the right-hand side expresses the probability for a collision specified by $\mathbf{v}'$, and $\mathbf{v}''$, $Nv\delta t d\sigma$, multiplied by the sum of the contributions to G of the two collision partners, and integrated over all possible collisions. The second term is the probability for not making a collision, multiplied by the contribution to G of a particle with unchanged speed, but changed initial position and starting time. After expansion of this equation in powers of δt, Eq. (5a) is obtained from the first-order terms.

We assumed two-body collisions between the atoms. An extension to many-body collisions would be easy if adequate expressions for the cross section were available. Note, however, that no assumption is made that two-body collisions are *elastic*. Thus, $d\sigma$ in Eq. (5a) is understood to contain electronic energy loss implicitly.

Equation (5a) applies to an ion of the same species as the target atoms. For the more general case of an arbitrary ion incident on a monatomic target we define an analogous function $G_{(1)}(x,\mathbf{v}_0,\mathbf{v},t)d^3\mathbf{v}_0dx$, which is the average number of *target* atoms moving as a consequence of an *ion* starting with $\mathbf{v}$ at $t=0$ in $x=0$. If the ion-target cross section is denoted by $d\sigma_{(1)}$, we immediately get

$$\frac{1}{v}\frac{\partial}{\partial t}G_{(1)}(x,\mathbf{v}_0,\mathbf{v},t)-\eta\frac{\partial}{\partial x}G_{(1)}(x,\mathbf{v}_0,\mathbf{v},t)$$
$$=N\int d\sigma_{(1)}[G_{(1)}(x,\mathbf{v}_0,\mathbf{v},t)$$
$$-G_{(1)}(x,\mathbf{v}_0,\mathbf{v}',t)-G(x,\mathbf{v}_0,\mathbf{v}'',t)],\quad(5b)$$

which is completely analogous to Eq. (5a), except that G and not $G_{(1)}$ represents the recoil term. Thus, Eq. (5a) can be solved only if G has been found from Eq. (5a).

In the following, we shall disregard the existence of a free surface in the calculation of $G(x,\mathbf{v}_0,\mathbf{v},t)$. The validity of this approximation depends on how often atoms are scattered back and forth through an imaginary surface in an infinite medium. This effect is assumed to be relatively unimportant when compared with slowing down of neutrons[27] and electrons,[36] because of the dominance of *soft* atomic collisions and rapid stopping as compared with the neutron case, and because of the more favorable mass ratio as compared with the electron case, all factors leading to more straightened-out particle trajectories. Already in case of electrons the effect appears to be small.[36]

In view of Eqs. (3) and (4), we are only interested in the function

$$F(x,\mathbf{v}_0,\mathbf{v})=\int_0^\infty G(x,\mathbf{v}_0,\mathbf{v})dt.\quad(6)$$

$F(x,\mathbf{v}_0,\mathbf{v})|v_{0x}|d^3v_0$ is the total number of atoms that penetrate the plane x with a velocity $(\mathbf{v}_0,d^3v_0)$ during the development of the collision cascade. $F(x,\mathbf{v}_0,\mathbf{v})$ satisfies an equation that follows from Eq. (5a) by integration over t:

$$\frac{1}{v}\delta(x)\delta(\mathbf{v}-\mathbf{v}_0)-\eta\frac{\partial}{\partial x}F(x,\mathbf{v}_0,\mathbf{v})=N\int d\sigma[F(x,\mathbf{v}_0,\mathbf{v})$$
$$-F(x,\mathbf{v}_0,\mathbf{v}')-F(x,\mathbf{v}_0,\mathbf{v}'')].\quad(7a)$$

Here we have assumed that

$$G(x,\mathbf{v}_0,\mathbf{v},t=0)=\delta(x)\delta(\mathbf{v}-\mathbf{v}_0),$$

representing *one* starting particle, and

$$G(x,\mathbf{v}_0,\mathbf{v},\infty)=0,$$

since at $t=\infty$, all atoms have slowed down below any finite velocity v_0. For an arbitrary ion we obtain similarly from Eq. (5b)

$$-\eta\frac{\partial}{\partial x}F_{(1)}(x,\mathbf{v}_0,\mathbf{v})=N\int d\sigma_{(1)}[F_{(1)}(x,\mathbf{v}_0,\mathbf{v})$$
$$-F_{(1)}(x,\mathbf{v}_0,\mathbf{v}')-F(x,\mathbf{v}_0,\mathbf{v}'')],\quad(7b)$$

where $F_{(1)}$ follows from $G_{(1)}$ by integration over t. Note that there is no source term, since at $t=0$ there are no moving *target* atoms.

3. EQUATIONS FOR SPUTTERING YIELD AND MOMENT EQUATIONS

Equations (7a) and (7b) are rather comprehensive but are not easy to solve, since there are seven variables. We will consider the general solutions in Paper II, but the present discussion will be restricted to the calculation of sputtering yields. According to Eqs. (3)

[36] L. V. Spencer, Phys. Rev. **98**, 1597 (1955).

and (6), the yield follows from Eq. (7a) by integration over $\mathbf{v}_0$, so that we get rid of three variables.

We consider only backward sputtering for the moment and introduce the functions

$$H(x,\mathbf{v})=\int d^3v_0\,|v_{0x}|\,F(x,\mathbf{v}_0,\mathbf{v}) \tag{8a}$$

and

$$H_{(1)}(x,\mathbf{v})=\int d^3v_0\,|v_{0x}|\,F_{(1)}(x,\mathbf{v}_0,\mathbf{v})\,, \tag{8b}$$

where the integrations over $\mathbf{v}_0$ obey the conditions

$$\eta_0=v_{0x}/v\leq 0\,, \tag{9}$$

$$E_0=\tfrac{1}{2}M_2v_0^2\geq U(\eta_0)\,, \tag{10}$$

and $U(\eta_0)$ is a surface binding energy that, in general, depends on the direction of ejection, characterized by the direction cosine η_0. We have introduced the common notation (Fig. 3)

$$\begin{aligned} M_1&=\text{mass of ion}\,,\\ M_2&=\text{mass of target atom}\,. \end{aligned} \tag{11}$$

The functions $H(x,\mathbf{v})$ and $H_{(1)}(x,\mathbf{v})$ represent the sputtering yields of a target atom or arbitrary ion, respectively, for the case that the source is at $x=0$ and the sputtered surface in the plane x. Thus, $H(x,\mathbf{v})$ are measurable in principle for $x\leq 0$. Since we actually deal with an infinite medium, these functions are also well defined for $x>0$.

We treat Eq. (7b) first. Multiplying both sides by $|v_{0x}|$ and integrating over $\mathbf{v}_0$ yields

$$\begin{aligned} -\delta(x)\eta\theta(-\eta)\theta(E-U(\eta))-\eta\frac{\partial}{\partial x}H(x,\mathbf{v})\\ =N\int d\sigma[H(x,\mathbf{v})-H(x,\mathbf{v}')-H(x,\mathbf{v}'')]\,, \end{aligned} \tag{12}$$

where E is the energy of the impinging particle,

$$E=\tfrac{1}{2}M_2v^2\,, \tag{13}$$

and

$$\begin{aligned} \theta(\xi)&=1, \quad \text{for } \xi>0\\ &=0, \quad \text{for } \xi<0\,. \end{aligned} \tag{14}$$

Obviously, in a random medium $H(x,\mathbf{v})$ will depend only on x, v, and η, the directional cosine, but not on the azimuth of $\mathbf{v}$ with respect to the x axis. Introducing energy instead of velocity variables, we finally obtain from Eq. (12)

$$\begin{aligned} -\delta(x)\eta\theta(-\eta)\theta(E-U(\eta))-\eta\frac{\partial}{\partial x}H(x,E,\eta)\\ =N\int d\sigma[H(x,E,\eta)-H(x,E',\eta')-H(x,E'',\eta'')]\,, \end{aligned} \tag{15}$$

where E', η', E'', and η'' are the energies and directional cosines (with respect to the x axis) of the scattered and recoiling particle, respectively. The sputtering yield is given by

$$S(E,\eta)=H(x=0,E,\eta)\,. \tag{16}$$

In the case of transmission sputtering, the source term in Eq. (15) reads $+\delta(x)\eta\theta(\eta)\theta[E-U(\eta)]$, and in Eq. (16) we have to set $x=d$ instead of $x=0$.

The standard procedure for solving this type of equation is to expand the angular dependence of H [and $H_{(1)}$] in terms of Legendre polynomials.[27] This expansion converges rapidly whenever the angular dependence of the function in question is relatively smooth. We know from experiment[1–3] that the sputtering yield does not show dramatic fluctuations as a function of η, at least for not too oblique incidence.[37,38] We expand

$$H(x,E,\eta)=\sum_{l=0}^{\infty}(2l+1)H_l(x,E)P_l(\eta)\,, \tag{17}$$

where $P_l(\eta)$ are Legendre polynomials. We then insert this expression into Eq. (15), and make the usual transformations,[22,25,27,36,39] to get the following set of equations for the coefficients $H_l(x,E)$:

$$\begin{aligned} \delta(x)Q_l(E)-\frac{\partial}{\partial x}[lH_{l-1}(x,E)+(l+1)H_{l+1}(x,E)]\\ =(2l+1)N\int d\sigma[H_l(x,E)-P_l(\cos\phi')H_l(x,E')\\ -P_l(\cos\phi')H_l(x,E'')]\,, \end{aligned} \tag{18}$$

where

$$Q_l(E)=\frac{2l+1}{2}\int_{-1}^{0}(-\eta)d\eta\theta(E-U(\eta))P_l(\eta) \tag{19}$$

and (Fig. 3) ϕ' is the laboratory scattering angle of scattered atom and ϕ'' is the laboratory scattering angle of recoiling atom. In case of transmission sputtering, $Q_l(E)$ has to be multiplied by $(-1)^l$.

It is customary and convenient to go over to moment equations, i.e., to multiply Eq. (18) by x^n ($n=0,1,2,\cdots$), integrate over x, and introduce the

---

[37] Recently, Evdokimov and Molchanov (Ref. 38) reported an oscillatory behavior of the sputtering yield as a function of the angle of incidence θ on polycrystalline samples. This deviation from monotonic increase with θ occurred at angles above about 70°, and the explanation proposed by the authors invokes a rearrangement of the surface layer of a polycrystal to form a close-packed plane. Thus, the assumption of random orientation of the crystallites is not valid, as far as the surface is concerned. The explanation of the effect is therefore outside the scope of random cascade theory. The possible rearrangement of the surface layer may play a role in the determination of surface binding forces and the angular distribution of sputtered atoms.

[38] I. N. Evdokimov and V. A. Molchanov, Can. J. Phys. **46**, 779 (1968).

[39] K. B. Winterbon, P. Sigmund, and J. B. Sanders, (unpublished).

moments

$$H_l^n(E)=\int_{-\infty}^{\infty} dx\, x^n H_l(x,E) \tag{20a}$$

and

$$H_{(1)l}^n(E)=\int_{-\infty}^{\infty} dx\, x^n H_{(1)l}(x,E). \tag{20b}$$

At the same time we separate elastic from inelastic (electronic) collisions by the scheme of Lindhard *et al.*[21,40] This yields

$$\begin{aligned}\delta_{n0}Q_l(E)&+n[lH_{l-1}^{n-1}(E)+(l+1)H_{l+1}^{n-1}(E)]\\ &=(2l+1)NS_e(E)\frac{d}{dE}H_l^n(E)+(2l+1)N\int_{T=0}^{E}d\sigma(E,T)\\ &\times[H_l^n(E)-P_l(\cos\phi')H_l^n(E-T)\\ &-P_l(\cos\phi'')H_l^n(T)],\end{aligned} \tag{21a}$$

and, by an analogous derivation,

$$\begin{aligned}n[lH_{(1)l-1}^{n-1}(E)&+(l+1)H_{(1)l+1}^{n-1}(E)]\\ &=(2l+1)NS_{(1)e}(E)\frac{d}{dE}H_{(1)l}^n(E)\\ &+(2l+1)N\int_{T=0}^{T_m}d\sigma_{(1)}(E,T)[H_{(1)l}^n(E)\\ &-P_l(\cos\phi')H_{(1)l}^n(E-T)-P_l(\cos\phi'')H_l^n(T)],\end{aligned} \tag{21b}$$

where $S_e(E)$ and $S_{(1)e}(E)$ are the electronic stopping cross sections, $d\sigma(E,T)$ and $d\sigma_{(1)}(E,T)$ are the differential cross sections for *elastic* scattering, T is the recoil energy, and

$$\begin{aligned}\cos\phi'&=(1-T/E)^{1/2}\\ &\quad+\tfrac{1}{2}(1-M_2/M_1)(T/E)(1-T/E)^{-1/2},\\ \cos\phi''&=(T/T_m)^{1/2},\\ T_m&=\gamma E,\\ \gamma&=4M_1M_2/(M_1+M_2)^2.\end{aligned}$$

Note that in Eq. (21a), $M_1=M_2$, so $\cos\phi'=(1-T/E)^{1/2}$ and $\cos\phi''=(T/E)^{1/2}$.

Moment equations are useful only when there is a procedure available to reconstruct a function of x from its moments. Distribution functions of the present type are often close to Gaussian shape, so that the Edgeworth expansion[41] in terms of Gaussians and derivatives of Gaussians may be useful. This has first been recognized by Baroody[42] and has been used successfully in both range theory,[22,25] radiation damage,[24,39] and sputtering.[28]

In deriving Eqs. (21a) and (21b), we neither introduced a bulk displacement threshold E_d nor a bulk binding energy V lost to the lattice by a recoiling atom. The latter quantity may not always be neglected, especially in covalent crystals. In those cases the recoil term $H_l^n(T)$ in Eqs. (21a) and (21b) has to be replaced by $H_l^n(T-V)$. Note, however, that in Refs. 5, 7, and 10, bulk binding energies had to be introduced since the yield would otherwise have been infinite. This indicates a basic inconsistency of these theories. Obviously, energy conservation requires that even for $E_d=0$ and $V=0$ only a finite number of atoms can penetrate to the surface and overcome the surface barrier. The competition between surface and bulk binding forces will be discussed in detail in II, since it shows up in the energy spectrum of sputtered atoms.

Isotropic sources. Examples of isotropic sources are radioactive atoms on the surface or in the bulk of a specimen, and recoils from elastic collisions caused by an isotropic flux of fast neutrons. The sputtering yield of a source located at $x=0$, with the surface in the plane x, is given by

$$S(x,E)=\frac{1}{2}\int_{-1}^{1}d\eta H(x,E,\eta)=H_0(x,E), \tag{22a}$$

by averaging Eq. (17) over all directions of recoil momentum. If recoil and target mass are different, we have

$$S_{(1)}(x,E)=H_{(1)0}(x,E). \tag{22b}$$

Thus, both $H_0(x,E)$ and $H_{(1)0}(x,E)$ are measurable quantities.

4. ANALYTIC SOLUTIONS

Before attacking the problem of solving Eqs. (21a) and (21b) we have to specify the input quantities S_e and $S_{(1)e}$, $d\sigma$ and $d\sigma_{(1)}$, and the surface binding energy $U(\eta_0)$. For analytic calculations we need simple expressions. Otherwise we have to solve the equations numerically.

A. Electronic Stopping

When needed, we use Lindhard's expressions[21,40]

$$S_e(E)=KE^{1/2},\quad S_{(1)e}(E)=K_{(1)}E^{1/2}, \tag{23a}$$

except when the ion velocity is so high that the Bethe-Bloch formula[43] applies. The latter can be approximated by

$$S_{(1)e}(E)=\text{const}/E. \tag{23b}$$

The constants K, $K_{(1)}$, and const depend on the atomic numbers and masses of ion and target.[21,43]

[40] J. Lindhard, V. Nielsen, M. Scharff, and P. V. Thomsen, Kgl. Danske Videnskab. Selskab, Mat.-Fys. Medd. **33**, No. 10 (1963).
[41] H. Cramer, *Mathematical Methods of Statistics* (Princeton University Press, Princeton, N. J., 1945).
[42] E. M. Baroody, J. Appl. Phys. **36**, 3565 (1965).
[43] H. A. Bethe, and J. Ashkin, in *Experimental Nuclear Physics*, edited by O. E. Segrè (John Wiley & Sons, New York, 1953), p. 166.

B. Cross Sections for Elastic Scattering

An especially useful choice is the power approximation of the Thomas-Fermi cross section,[20] where

$$d\sigma = CE^{-m}T^{-1-m}dT, \tag{24a}$$

$$d\sigma_{(1)} = C_{(1)}E^{-m}T^{-1-m}dT, \tag{24b}$$

and m is a number between 0 and 1. $m=1$ holds for Rutherford scattering. Over a major portion of the keV range and for medium-mass ions and atoms, $m=\frac{1}{2}$ is a fair approximation, while in the lower-keV and upper-eV region, $m=\frac{1}{3}$ should be adequate. In the eV region where the Thomas-Fermi potential overestimates the interaction, a Born-Mayer potential may be appropriate, but even in this case, Eq. (24a) may be a reasonable approximation if m is taken close to zero.[44]

The constants C and $C_{(1)}$ are given by[20]

$$C = \tfrac{1}{2}\pi\lambda_m a_{22}^2(2Z_2^2e^2/a_{22})^{2m}, \tag{25a}$$

$$C_{(1)} = \tfrac{1}{2}\pi\lambda_m a_{12}^2(M_1/M_2)^m(2Z_1Z_2e^2/a_{12})^{2m}, \tag{25b}$$

where Z_1 and Z_2 are atomic numbers, a_{12} and a_{22} are Thomas-Fermi screening radii, and λ_m are dimensionless constants equal to[20,39]

$$\lambda_1 = 0.5, \quad \lambda_{1/2} = 0.327, \quad \lambda_{1/3} = 1.309. \tag{26}$$

It will be convenient in the following also to characterize collisions in the eV range by a power cross section. For $m=0$ we get from Eqs. (24a) and (24b)

$$d\sigma = CdT/T, \quad d\sigma_{(1)} = C_{(1)}dT/T, \tag{27}$$

and, if Eqs. (25a) and (25b) were assumed to remain valid,

$$C = \tfrac{1}{2}\pi\lambda_0 a_{22}^2, \quad C_{(1)} = \tfrac{1}{2}\pi\lambda_0 a_{12}^2. \tag{28}$$

Figure 4 shows a "Lindhard plot" of the cross section (27) and that following from Born-Mayer interaction between two atoms

$$V(r) = Ae^{-r/a}, \tag{29}$$

where r is the distance between the nuclei, A is a constant, and a is the screening radius. Andersen and the present author[45] proposed

$$A = 52(Z_1Z_2)^{3/4}\ \text{eV}, \quad a = 0.219\ \text{Å}. \tag{30}$$

Classical scattering angles for the potential (29) have been computed by Robinson,[46] and the curves in Fig. 4 were found by numerical differentiation and plotting the function

$$f(t^{1/2}) = \frac{2t^{3/2}}{\pi a^2}\frac{d\sigma}{dt}, \tag{31a}$$

where

$$t = \epsilon^2 T/T_m \tag{31b}$$

and

$$\epsilon = \frac{M_2}{M_1+M_2}\frac{E}{A}. \tag{31c}$$

The Born-Mayer cross sections do not reveal quite as nice "similarity" properties as Thomas-Fermi cross sections,[20] i.e., the $f(t^{1/2})$ curves do not coincide for different values of ϵ. At high ϵ energies, though, the curves appear to converge toward a dependence $f(t^{1/2}) = 7.35t^{0.445}$ that is equivalent to Eq. (24a) with $m=0.055$. This value of m is indeed very close to zero. Unfortunately the Born-Mayer cross section will be needed at very small ϵ where this asymptotic formula would not be too accurate. The energies of interest go well below $\epsilon=0.005$, the smallest energy for which cross sections have been tabulated.[46]

At these energies, the validity of most existing potentials becomes questionable, and so does the concept of two-particle collisions. We choose the form (27) that leads to $f(t^{1/2}) = \lambda_0 t^{1/2}$, first of all because of its simplicity. For $\lambda_0 = 24$ (dashed curve in Fig. 4) one obtains a reasonable over-all fit at the lowest ϵ energies. Note especially that the constant A in Eq. (29) does not enter the cross section. This removes a major ambiguity, since A values for the same elements, as given by different authors, differ by as much as several orders of magnitude.[45] For the purpose of numerical evaluations we replace Eq. (28) by

$$C_0 = \tfrac{1}{2}\pi\lambda_0 a^2, \quad \lambda_0 = 24, \quad a = 0.219\ \text{Å}, \tag{28'}$$

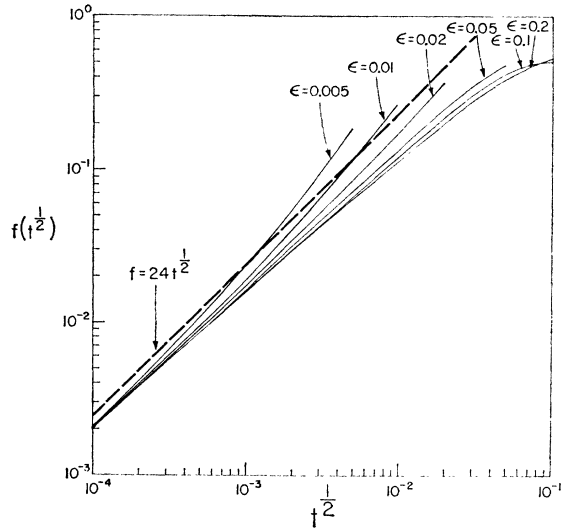

FIG. 4. Comparison between differential cross sections for Born-Mayer interaction (solid curves) and Eq. (27) (dashed curve). $f(t^{1/2})$, t, and ϵ are defined in Eqs. (31a)–(31c).

[44] P. Sigmund and P. Vajda, Danish Atomic Energy Commission Risö Report Nos. 83 and 84, 1964 (unpublished).

[45] H. H. Andersen and P. Sigmund, Nucl. Instr. Methods **38** 238 (1965); Danish Atomic Energy Commission Risö Report No. 103, 1965 (unpublished).

[46] M. T. Robinson, Oak Ridge National Laboratory Report No. ORNL-3493, 1963 (unpublished).

in view of Eq. (30). From Eqs. (27) and (28′) we obtain the center-of-mass scattering angle χ as a function of impact parameter p,

$$\sin\tfrac{1}{2}\chi=\exp(-p^2/\lambda_0 a^2), \tag{32}$$

i.e., heavy deflection for $p\ll a\sqrt{\lambda_0}$ and small deflection for $p\gg a\sqrt{\lambda_0}$. The critical impact parameter $a\sqrt{\lambda_0}$ is about 1 Å, i.e., of the order of an atomic radius. Robinson[47] has reconstructed the "potential" underlying the scattering law (32) and concluded that the variation with energy and the deviation from exponential shape remain with the uncertainty of the potential (29).

Apart from the differential cross sections, we need the elastic stopping powers

$$S_n(E)=\int_0^E T d\sigma=\frac{1}{1-m}CE^{1-2m} \tag{33a}$$

and

$$S_{(1)n}(E)=\int_0^{T_m} T d\sigma_{(1)}=\frac{1}{1-m}C_{(1)}\gamma^{1-m}E^{1-2m}. \tag{33b}$$

These expressions can be used to define rough energy limits within which cross sections for various values of m apply, especially the limiting energy E^* up to which the cross section with $m=0$ is feasible. For $E>E^*$, we assume that $m=\frac{1}{3}$, so

$$E^*=\left(\frac{3\lambda_{1/3}}{2\lambda_0}\right)^{3/2}\frac{M_1+M_2}{M_2}\left(\frac{a_{12}}{a}\right)^3\frac{Z_1Z_2e^2}{a_{12}}, \tag{34}$$

where E^* is of the order of some hundred eV.

For $m=0$, the stopping powers (33a) and (33b) become proportional to energy, so that, for example, the total range of an ion or atom diverges. This will not introduce any divergencies into the sputtering calculation, but to make sure that no drastic over- or underestimate of the sputtering yield is made, one might prefer to use a low-energy cross section with a finite value of $m\approx 0.05$, as suggested by Fig. 4. Such a calculation has been done, and the resulting change in the absolute magnitude of the sputtering yield is measurable, but small compared with the uncertainty introduced by the lack of knowledge of surface binding conditions.

C. Surface Binding Forces

Both the magnitude and the angular variation of the surface binding energy deserve careful consideration. Obviously, introduction of a bulk displacement energy $E_d\approx 25$ eV and neglect of a surface binding energy[5,7,10,48] must falsify the energy spectrum. There is little doubt that atoms may be ejected at very few eV. In some theories, surface binding was contained implicitly in more comprehensive fitting parameters.[6,9,15] The problem received attention in computer simulations of sputtering,[14,35] and Thompson[12] pointed out that the angular distribution of sputtered particles may be sensitive to $U(\eta_0)$. In single-crystal sputtering, $U(\eta_0)$ is one of the factors that determine the shape of spot patterns.[16]

There is little first-hand information available about $U(\eta_0)$. Evaporation data cannot be used tacitly in sputtering, since evaporation appears to take place from preferred positions, and since the energy necessary for an atom to ultimately leave the surface is probably transferred to this atom in several steps.[49] Possibilities to determine $U(\eta_0)$ from sputtering experiments will be discussed in II.

Two basically simple surface conditions have been used in previous theories. The first is the planar potential barrier or work-function model, leading to

$$U(\eta_0)=U_0/\eta_0^2, \tag{35}$$

since the energy component perpendicular to the surface must be greater than the barrier height U_0, in order that an atom can be ejected. The second is a spherically potential barrier[35]

$$U(\eta_0)=U_0. \tag{36}$$

While Eq. (35) is well established in many emission phenomena, the author feels that its use in sputtering is not justified without comment, despite frequent use (for a review, see Ref. 35).

As an example, we consider the ejection of a surface atom. $U(\eta_0)$ is determined by the cohesive forces provided by neighboring atoms and conduction electrons. Let us assume a simplified lattice model with only two-body interactions between nearest-neighbor atoms and, to be specific, consider the (100) surface of an fcc crystal. We take the interatomic potential around the equilibrium distance,

$$V(r_{ij})=-V_0+f(r_{ij}-D)^2, \tag{37a}$$

where V_0 is the bond strength, f the force constant, and D the nearest-neighbor distance. For nearest-neighbor interaction this lattice is stable, even at the surface. Note that the cohesive energy is $6V_0$ per atom[50] and not $12V_0$, as stated in Ref. 35. The surface atom in question has the equilibrium position $x=y=z=0$ (Fig. 5). If the atom is part of an ideal surface, its eight nearest neighbors (1–8) make up a potential in the harmonic region,

$$W(x,y,z)=-8V_0+f(2x^2+3y^2+3z^2), \tag{37b}$$

where x is the direction perpendicular to the surface.

[47] M. T. Robinson (private communication).

[48] P. V. Pavlov, D. I. Tetel'baum, E. I. Zorin, and V. I. Alekseev, Fiz. Tverd, Tela 8, 2679 (1966) [English transl.: Soviet Phys.—Solid State 8, 2141 (1967)].

[49] G. A. Somorjai and J. E. Lester, Progr. Solid State Chem. 4, 1 (1967).

[50] R. M. J. Cotterill and M. Doyama, in *Lattice Defects and Their Interactions*, edited by R. R. Hasiguti (Gordon and Breach, Science Publishers, Inc., 1967), p. 1.

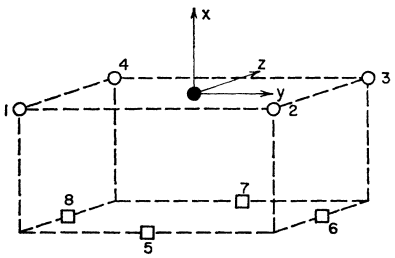

FIG. 5. Geometry of ejection process; (100) surface of fcc crystal.

$W(x,y,z)$ is the potential acting on an atom moving away from its equilibrium position, provided that the neighbors *keep at rest.* The interesting feature of Eq. (37b) is that the force constant is *smallest* in the x direction, which is in contrast to the assumption of a planar potential barrier.

In a sputtering experiment, the surface will usually be far from ideal. Let us neglect deformations, interstitials, etc., and just look at $W(x,y,z)$ for the case that one or more of the four nearest neighbors in the surface (atoms 1–4 in Fig. 5) have been removed. We obtain: one neighbor removed:

$$W(x,y,z)=-7V_0+f(2x^2+\tfrac{5}{2}y^2+\tfrac{5}{2}z^2\pm yz); \quad (37c)$$

two adjacent neighbors removed:

$$W(x,y,z)=-6V_0+f(2x^2+2y^2+2z^2); \quad (37d)$$

two opposite neighbors removed:

$$W(x,y,z)=-6V_0+f(2x^2+2y^2+2z^2\pm 2yz); \quad (37e)$$

three neighbors removed:

$$W(x,y,z)=-5V_0+f(2x^2+\tfrac{3}{2}y^2+\tfrac{3}{2}z^2\pm yz); \quad (37f)$$

four neighbors removed:

$$W(x,y,z)=-4V_0+f(2x^2+y^2+z^2). \quad (37g)$$

In Eq. (37g), the atom is located on top of an ideal surface, like an adsorbed atom. The potential barrier decreases from $8V_0$ in Eq. (37b) to half that value in Eq. (37g), and the force constant becomes *relatively* greater in the x direction from Eq. (37b) down through Eq. (37g).

Equations (37) should not be overinterpreted. Obviously, all the simplifications made in the derivation tend to eliminate the more collective part of surface binding forces, such that Eq. (36) seemed more appropriate than Eq. (35). But we want to make the following conclusions:

(1) Equation (35) is not as accurate—and Eq. (36) not as unphysical—as one might suspect.

(2) There will, in general, be a *distribution* of binding energies U_0.

(3) The average surface binding energy may depend slightly on the crystal surface considered and on the state of damage of the surface. This might explain part of the observed dose dependence of the sputtering yield,[1] but may interfere with other dose effects.

We shall go into more details—such as investigating other crystallographic surfaces—since this model cannot in any respect compete with a careful computer simulation of the ejection process. Such a study is being done.[51] Note that atomic binding forces were not included in any of the previous computer simulations of sputtering.[14,35,48,52]

In the following, we assume that the most realistic expression is indeed Eq. (35), at least for metals, with U_0 equal to the cohesive energy per atom or the measured sublimation energy. But in order to check the sensitivity of the sputtering yield to $U(\eta_0)$ we make a parallel calculation with Eq. (36).

D. Zero-Order Moments

This subsection and the following one are devoted to the solution of Eqs. (21a) and (21b) with the input quantities introduced in the two previous paragraphs. While the complete solutions would be difficult to obtain, and would not be convenient for further use, it turns out that only very few of the $H_l^n(E)$ are significant in the limit of high ion energies, i.e., $E\gg U_0$. Since U_0 is of the order of a few eV, we have to assume that E is greater than 100–200 eV. Hence, sputtering near threshold is excluded from consideration. The assumption that $E\gg U_0$ will be applied consistently, and only the terms with the highest power of E/U_0 will be taken into account in each order n. Equations (21a) and (21b) have not been treated previously in connection with ion slowing down, but they are similar to other sets of equations that have been solved by use of power cross sections.[21–25,39,40,53,54] The key reference is the thesis of Sanders,[22] but contrary to Sanders, we calculate *exact* asymptotic solutions that are found by Laplace transform.[23]

For $n=0$, Eq. (21a) reads

$$Q_l(E)=(2l+1)NCE^{-m}\int_0^E \frac{dT}{T^{1+m}} \times[H_l^0(E)-P_l((1-T/E)^{1/2})H_l^0(E-T) -P_l((T/E)^{1/2})H_l^0(T)], \quad (38)$$

where we assumed $S_e(E)=0$ for the moment, and inserted $d\sigma$ from Eq. (24a). With surface binding from Eq. (35), we obtain the following expressions for the

[51] D. Jackson (in preparation).
[52] D. T. Goldman, D. E. Harrison, and R. R. Coveyou, Oak Ridge National Laboratory Report No. ORNL-2729, 1959 (unpublished).
[53] J. B. Sanders, Physica 32, 2197 (1966).
[54] P. Sigmund, Radiation Effects 1, 15 (1969).

source terms (19):

$$Q_0(E)=\tfrac{1}{4}(1-U_0/E), \tag{39a}$$

$$Q_1(E)=\tfrac{1}{2}[-1+(U_0/E)^{3/2}], \tag{39b}$$

$$Q_2(E)=(5/16)[1+2U_0/E-3(U_0/E)^2], \tag{39c}$$

$$Q_3(E)=(7/4)[-(U_0/E)^{3/2}+(U_0/E)^{5/2}]. \tag{39d}$$

Equations (39a)–(39d) hold for $E\geq U_0$. For $E<U_0$, we have $Q_l(E)=0$ and hence

$$H_l^0(E)=0, \quad \text{for } E<U_0. \tag{40}$$

Equation (40) is trivial but important for the mathematical solution of Eq. (38).

With the alternative surface binding condition (36), we would retain only those terms that are independent of U_0/E in Eqs. (39a)–(39d).

The procedure of determining the leading terms of an asymptotic expansion in powers of E has been described in great detail by Robinson[23] on the example of the Kinchin-Pease equation of radiation damage theory. Therefore, we only present the results of our calculation, which is straightforward but somewhat lengthy. Writing only terms with positive powers of E, we arrive at the expressions

$$H_0^0(E)\sim\frac{1}{\psi(1)-\psi(1-m)}\frac{m}{1-2m}\frac{E}{8NCU_0^{1-2m}}+\frac{1}{-1/m-B(-m,2m)}\frac{E^{2m}}{8NC}, \tag{41a}$$

$$H_1^0(E)\sim\frac{-1}{\psi(1)-\psi(1-m)}\frac{m}{1-4m}\frac{E^{1/2}}{4NCU_0^{1/2-2m}}+\frac{1}{1/m+2/(1+2m)+B(-m,\frac{3}{2}+2m)}\frac{E^{2m}}{6NC}, \tag{41b}$$

$$H_2^0(E)\sim-\frac{1}{1/m+3/(1+m)+3B(-m,2+2m)+2B(1-m,2m)}\frac{E^{2m}}{8NC}, \tag{41c}$$

$$H_3^0(E)\sim 0. \tag{41d}$$

The functions $B(\xi,\eta)$ and $\psi(\xi)$ are the β function and the digamma function

$$B(\xi,\eta)=\Gamma(\xi)\Gamma(\eta)/\Gamma(\xi+\eta), \tag{42a}$$

$$\psi(\xi)=(d/d\xi)\ln\Gamma(\xi). \tag{42b}$$

Which of the expressions in Eqs. (41a)–(41c) is the leading one depends on the value of m. For $m=0$, i.e., $E<E^*$, we obtain

$$H_0^0(E)\sim\frac{1}{8\psi'(1)}\frac{E}{NC_0U_0}, \tag{43a}$$

$$H_1^0(E)\sim-\frac{1}{4\psi'(1)}\frac{E^{1/2}}{NC_0U_0^{1/2}}, \tag{43b}$$

$$H_2^0(E)\sim H_3^0(E), \tag{43c}$$

$$\sim 0, \tag{43d}$$

where C_0 is given by Eq. (28′), and

$$\psi'(\xi)=(d/d\xi)\psi(\xi), \quad \psi'(1)=\tfrac{1}{6}\pi^2. \tag{44}$$

The constant terms were dropped in Eqs. (43a)–(43d). Obviously, the term $H_0^0(E)$ is leading, and the only one to be taken into account for $m=0$.

It is a very central point of the calculation that the term $H_0^0(E)$ is leading at *all* energies $E\gg U_0$, and that it has the same asymptotic form, Eq. (43a), i.e., that we have to insert $m=0$, even at energies $E>E^*$, where the scattering of the ion is governed by a cross section with $m\geq\frac{1}{3}$. Both a physical and a mathematical argument are presented to prove this point.

Let us first discuss the meaning of the moment $H_0^0(E)$. According to Eq. (22a), the function $H_0(x,E)$ determines the sputtering yield from a surface in x of an isotropic source located in $x=0$. According to Eq. (20a), the moment $H_0^0(E)$ is the integral of $H_0(x,E)$ over all x, i.e., determines the number of atoms penetrating a plane at an arbitrary position x with a certain minimum energy, when there is a *homogeneous* isotropic source of recoiling atoms throughout an *infinite* medium.

The first term in $H_0^0(E)$, according to Eq. (41a), is proportional to $(E/U_0)(U_0^{2m}/NC)$, where E/U_0 is, roughly, the number of atoms per ion that is set in motion with an energy greater than U_0, and U_0^{2m}/NC is, apart from a factor, the range of an atom with energy U_0. Obviously, the latter quantity is determined by the scattering law valid at $E=U_0$, i.e., $m=0$, while the former quantity is insensitive to the scattering law of the high-energy ions.

The second term in Eq. (41a) is proportional to E^{2m}/NC, which is the range of a particle of energy E, apart from a factor. This term obviously determines the probability that the ion itself penetrates the plane under consideration. Hence, one has to insert those values of m and C that are appropriate at the energy E. For $m\geq\frac{1}{2}$, the second term could compete with the first one. Numerically, however, the second term is negligibly small. Let us assume a medium mass target so that the range E^{2m}/NC is of the order of 100 Å at

100 keV where $m=\frac{1}{2}$. The range $(U_0^{2m}/NC)_{m=0}$ is of the order of 1 Å, while the factor E/U_0 is about 10^4–10^5. Thus, the ratio between the two competing terms is about 100–1000, and does not depend on E for $m=\frac{1}{2}$. At high energies, inelasticity reduces both terms, while at lower energies the situation of Eq. (43a) is approached.

Once the second term in Eq. (41a) is neglected, we also have to drop the second term in Eq. (41b). The first term in Eq. (41b) must be dropped since it is smaller by a factor of $(U_0/E)^{1/2}$ than the leading term. Similar considerations apply to the moments for $l\geq 2$.

The observation may be of interest that quantities characterizing *low-energy* recoils (C_0,U_0) enter only the terms $H_0^0(E)$ and $H_1^0(E)$, while quantities characterizing the *ion* enter both $H_0^0(E)$, $H_1^0(E)$, $H_2^0(E)$, and some of the higher moments $H_l^0(E)$. This is related to the fact that the velocity distribution of low-energy recoils is essentially isotropic, apart from a weak anisotropy required by momentum conservation[22] and expressed in the $l=1$ term, while the velocity distribution of the ion is anisotropic during the slowing-down process.

The second proof of Eq. (43a) for $m>0$ is is purely mathematical. Let us consider the last integral in Eq. (38) for $l=0$, i.e.,

$$\int_{U_0}^{E}\frac{dT}{T^{1+m}}H_0^0(T).$$

For $E>E^*$, we have $m=\frac{1}{3}$. The integral is split up into the region $U_0\leq T\leq E^*$, where $H_0^0(T)$ is known from Eq. (43a), and the region $E^*\leq T\leq E$, where $H_0^0(T)$ is unknown. The second integral in Eq. (38) is split up in a similar way. The method of Laplace transform can then be applied to calculate the asymptotic solutions of Eq. (38) for $E\gg E^*$. The calculation is straightforward and completely analogous to a previous one on the Kinchin-Pease equation.[54] As a result, one obtains Eq. (43a) as the leading term of the asymptotic expansion.

None of the considerations in this subsection is bound to the assumption that m is *exactly* equal to zero at small energies. Should m be slightly greater than zero, the expression for $H_0^0(E)$ has to be calculated from Eq. (41a).

When $H_0^0(E)$ is determined on the basis of the surface binding condition (36) instead of (35), one obtains *twice* the value given in Eq. (43a). This doubles the calculated sputtering yield.

The effect of electronic stopping $S_e(E)$ on $H_0^0(E)$ is readily included. Since $H_0^0(E)$ is proportional to E, for elastic scattering, and since the integrand in Eq. (38) for $l=0$ has the form discussed by Lindhard *et al.*,[40] we can take over their result and replace E by $\nu(E)$, so that

$$H_0^0(E)=\frac{1}{8\psi'(1)}\frac{\nu(E)}{NC_0U_0}, \tag{45}$$

where $\nu(E)/E$ is the fraction of the energy that is not lost to ionization during the slowing-down process. Both analytic and numerical estimates of this function are available for $M_1=M_2$.[40]

We now consider the solutions of Eq. (21b) for $M_1\neq M_2$. For $n=l=0$ and $S_{(1)e}(E)=0$, Eq. (22b) reads

$$0=\int d\sigma_{(1)}[H_{(1)0}^0(E)-H_{(1)0}^0(E-T)-H_0^0(T)]. \tag{46a}$$

Inserting $H_0^0(E)$ from Eq. (43a), and neglecting the condition

$$H_{(1)l}^0(E)=0, \quad \text{for } E<U_0 \tag{46b}$$

that follows from Eq. (40), the linearity of $H_0^0(E)$ with E shows that

$$H_{(1)0}^0(E)=H_0^0(E) \tag{47a}$$

must be the solution of Eq. (46a), independent of the form of $d\sigma_{(1)}$. By inserting $d\sigma_{(1)}$ from Eq. (24b), and getting proper solutions by taking into account Eqs. (40) and (46b), one arrives at the result that Eq. (47a) is exact in the highest order in E.

When electronic stopping is included (i.e., S_e in H_0^0 and $S_{(1)e}$ in $H_{(1)0}^0$), one can again take over the results of Lindhard *et al.*,[40] so that

$$H_{(1)0}^0(E)=\frac{1}{8\psi'(1)}\frac{\nu_{(1)}(E)}{NC_0U_0}. \tag{47b}$$

The function $\nu_{(1)}(E)$ has been calculated for a few examples,[40] and a computer code exists at Aarhus University that can tabulate $\nu_{(1)}(E)$ for any desired ion-target combination. Both $\nu(E)$ and $\nu_{(1)}(E)$ were calculated on the basis of the comprehensive Thomas-Fermi cross section rather than the power cross sections, Eqs. (24a) and (24b). It is both justified and consistent to use these results in the present connection, since the cross section for high-energy ions—for which electronic stopping is important—does not enter Eq. (43a).

Finally, we have to estimate the effect of a bulk binding energy V on the solutions of Eq. (38). As mentioned previously, the recoil term $H_l^0(T)$ has to be replaced by $H_l^0(T-V)$. Direct solution of Eq. (38) is not very convenient, then. An easier way is to go over the velocity distribution function $F(x,\mathbf{v}_0,\mathbf{v})$ defined in Eq. (6). This function will be of central interest in II, and since we will not make much use of $H_0^0(E)$ for $V\neq 0$ in the present paper, we only mention the results and refer to II for a derivation. Keeping the surface binding condition (35), one has to make the following

substitution in Eqs. (43a), (45), and (47b):

$$\frac{1}{U_0}\rightarrow\frac{1}{V}\left[\left(1+\frac{U_0}{2V}\right)\ln\left(1+\frac{2V}{U_0}\right)-1\right]. \quad (48a)$$

With the surface binding condition (36), the proper substitution is

$$1/U_0\rightarrow(1/V)\ln(1+2V/U_0). \quad (48b)$$

Both expressions are exact for $V\ll U_0$ and very accurate for $V\lesssim 2U_0$, while they are inaccurate for $V\gg 2U_0$.

E. Higher Moments, General Sputtering-Yield Formula, and Depth of Origin of Sputtered Atoms

With the substitution

$$H_l^n(E)=(3/4\pi^2)(NC_0U_0)^{-1}F_l^n(E), \quad (49)$$

Eq. (21a) reads for, $n\geq 1$,

$$nlF_{l-1}^{n-1}(E)+n(l+1)F_{l+1}^{n-1}(E)$$
$$=(2l+1)NS_e(E)\frac{d}{dE}F_l^n(E)+(2l+1)N\int d\sigma$$
$$\times[F_l^n(E)-P_l(\cos\phi')F_l^n(E-T)$$
$$-P_l(\cos\phi')F_l^n(T)], \quad (50a)$$

and from Eqs. (44) and (45)

$$F_l^0(E)=\delta_{l0}\nu(E). \quad (50b)$$

Equations (50a) and (50b) determine moments of the depth distribution of deposited energy $F(x,E,\eta)$, where $F(x,E,\eta)dx$ is the amount of energy deposited in a layer (x,dx) by an ion of energy E starting in $x=0$, and all generations of recoil atoms. Equation (50b) is the normalization

$$\int_{-\infty}^{\infty}dxF(x,E,\eta)=\nu(E). \quad (50c)$$

The function $F(x,E,\eta)$ has been introduced in Ref. 24, with the slight difference that the *vector* distribution was considered there, while we deal with the *depth* distribution here. This causes different coefficients of F_{l-1}^{n-1} and F_{l+1}^{n-1} on the left-hand side of Eq. (50a). The two distributions can be transformed into each other, and an extensive study of both distributions for elastic scattering $[\nu(E)\equiv E]$ is being finished.[39] Averages $\langle x^n\rangle$ for $n=1$, 2, and 3 over F have been published for elastic scattering,[24] and distribution functions have been reconstructed from the averages.[28] Hence, we only discuss those features of F that are important for the understanding of the present applications. For details the reader is referred to Refs. 24 and 39.

The most important property of F is that it depends only on the slowing-down characteristics of the primary particle and high-energy recoil atoms. The depth distribution of deposited energy extends over a distance of the order of the ion range. Therefore, it is not influenced by the ranges of low-energy recoils. For the same reason, one is justified in neglecting the cutoff energy U_0 that arises from Eq. (40) in the integral equation (50a) and in neglecting the bulk binding energy V in the recoil term $F_l^n(T)$. Asymptotic expansion for large E of the correct equations[22,39] shows that neither U_0 nor V enters the highest terms.

Going back from the moments in Eq. (49) to the distribution function, we obtain

$$H(x,E,\eta)=\frac{3}{4\pi^2}\frac{F(x,E,\eta)}{NC_0U_0}, \quad (51a)$$

and from Eqs. (21b), (47a), and (47b),

$$H_{(1)}(x,E,\eta)=\frac{3}{4\pi^2}\frac{F_{(1)}(x,E,\eta)}{NC_0U_0}, \quad (51b)$$

where $F_{(1)}(x,E,\eta)$ is the deposited energy distribution for $M_1\neq M_2$. Also, this function is known from previous work.[24,39] H and $H_{(1)}$ as given in Eqs. (51a) and (51b) determine the sputtering yield for a surface at x and a source at $x=0$. The orientation of the surface (backward or forward sputtering) does not make any difference, since only the $l=0$ term was taken into account in the zero-order moments.

We now rederive the sputtering-yield formula (51a) on a more qualitative basis that makes clear the various steps that make up the sputtering process. The argument also holds for Eq. (51b).

(1) During the slowing down of the ion and energetic recoil atoms, a certain amount of energy $F(x,E,\eta)dx$ is deposited in a layer (x,dx) near the surface of the target. This energy is bound to remain in this region, since it is stored in kinetic energy of very slowly moving atoms.

(2) The number of low-energy atoms that are set in motion with an energy (E_0,dE_0) follows from the *recoil density*[55] by multiplying the amount of energy available with a factor

$$\frac{m}{\psi(1)-\psi(1-m)}\frac{dE_0}{E_0^2}.$$

Hence, for $m=0$, the expression

$$\frac{6}{\pi^2}\frac{F(x,E,\eta)}{E_0^2}dE_0dx, \quad E_0\ll E \quad (52)$$

gives the number of atoms recoiling with an energy (E_0,dE_0) in a layer (x,dx).

[55] P. Sigmund, Appl. Phys. Letters 14, 114 (1969).

(3) Half of these atoms move toward the surface, and their velocity distribution is isotropic for $E_0 \ll E$. The number of atoms that *initially* have energy enough to overcome the surface barrier is found by integrating Eq. (52) and taking into account the surface binding condition $E_0 \geq U(\eta_0)$, Eq. (35). This yields

$$\frac{1}{\pi^2}\frac{F(x,E,\eta)}{U_0}dx \tag{53}$$

atoms that satisfy the conditions for sputtering initially.

(4) If the depth Δx from which the sputtered particles come is small, one may neglect the loss of energy between the points of origin and the surface. Then, the sputtering yield becomes

$$H(x,E,\eta)=\frac{1}{\pi^2}\frac{F(x,E,\eta)}{U_0}\Delta x. \tag{54}$$

Comparing this expression with Eq. (51a), we obtain

$$\Delta x=\tfrac{3}{4}(1/NC_0) \tag{55}$$

for the effective depth of origin of the sputtered atoms.

From Eq. (28′) one obtains $\Delta x = 4.8$ Å for copper. Note that, as it stands, Δx depends only on the density of the target. When the energy loss between the point of origin and the surface is not neglected, one obtains a slightly larger value for Δx.

F. General Yield Formula

Equations (51a) and (51b) make possible a clear distinction between those features of the sputtering yield that can be predicted with good accuracy from collision theory and other features where one would expect uncertainties.

The function $F(x,E,\eta)$ is determined by Eqs. (50a) and (50b), which require electronic stopping and the differential cross section as input quantities. Except for the case where the *ion* energy is in the eV range, both quantities are known with reasonable accuracy, and current experimental and theoretical work will certainly clarify some of the open questions in the near future. Also, the assumptions of two-particle scattering and random slowing down are justified, unless bombardment is done under channeling conditions. Therefore, the problem of determining $F(x,E,\eta)$ is reduced to the purely mathematical problem of solving Eq. (50a) and reconstructing the function from its moments, preferably by dropping the assumption of an infinite medium and introducing a surface without binding forces.[28] At least for elastic collisions, the problem of calculating $F(x,E,\eta)$ has been solved with reasonable accuracy,[24,28,39] but only for an infinite medium. These results will be used in Sec. 4 G. For inelastic collisions, Eq. (50a) has to be solved numerically, except in some simple cases that will be discussed below. The coding is being done, but no results are available yet.

Assuming that F and $F_{(1)}$ can be calculated properly, one concludes from Eqs. (51a) and (51b) that the dependence of the sputtering yield on ion *type*, *energy*, and *angle of incidence* and the relation between *backward* and *transmission* sputtering ($x=0$ or d) can be predicted accurately by collision theory.

The other quantities occurring in Eq. (51a) characterize the *target* only. The following uncertainties should be mentioned:

(a) The assumptions of random slowing down and of binary collisions may break down at low energies. There may be a small contribution from focused collision sequences. The quantitative effect on the sputtering yield will depend on the target.

(b) The rather uncertain low-energy cross section as defined by Eqs. (27) and (28′) affects the numerical factor in front of Eq. (51a), the value of C_0 (that may depend on the target), and the accurate dependence on U_0.

(c) The surface binding condition (35) affects the numerical factor in front of Eq. (51a); the value of U_0 is not known from first principles but determines the magnitude of the yield. Further uncertainties arise when a bulk binding energy is introduced [Eqs. (48a) and (48b)].

(d) Also, the assumption of a planar surface may influence the magnitude of the yield. So long as surface roughness is on a scale that is small compared to the dimensions of the cascades, its effect on the sputtering yield will often average out. Surface roughness on a larger scale, however, will tend to increase the yield. The quantitative effect depends on the geometry and can be estimated when the shape of the surface is known.

(e) The assumption of an infinite medium may also affect the flux of low-energy recoils.

There is no way at present of getting an estimate of the cumulative uncertainty from the above points, but one has to expect an *a priori* uncertainty of at least a factor of 2 in either direction. On the other hand, it will turn out that in almost all those cases where measurements done by several groups provided reliable sputtering ratios, the *apparent* accuracy of Eqs. (51a) and (51b) is much better ($\sim$20–30%). This good agreement is *not* achieved by adjusting any of the available input parameters, but may be due to cancellation of errors. Possible procedures to determine the material factor $(3/4\pi^2)/NC_0U_0$ accurately will be discussed in Sec. 5 A.

G. Relation to Previous Theories

Qualitative arguments of the type discussed in Sec. 4 E have been used previously to derive yield formulas.[5,7] Because of the introduction of bulk instead of surface binding energies ($E_d \approx 25$ eV, $U_0 \approx 3$ eV for noble metals), the number of atoms set in motion was

relatively small. Therefore, in fitting experimental sputtering yields, one had to assume rather long "diffusion" paths of the atoms prior to ejection. Brandt and Lambert,[10] in an elaborate mathematical treatment, also introduced bulk binding energies, and furthermore described the stopping of low-energy recoils by the Thomas-Fermi cross section[20] that yields much *smaller* stopping distances in the 10–100-eV range than the low-energy cross section used in the present work. One would expect, therfore, that the final yield formula of Brandt and Lambert underestimates the sputtering yield by at least an order of magnitude but, in fact, their yield formula shows good agreement with some experimental data. The author was unable to trace out which additional assumption in the theory canceled this discrepancy.

More or less explicitly, many theories of sputtering by ion beams[5,7–10,12,13,15,19] assumed that only the first collision undergone by the ion gives rise to a cascade that eventually leads to sputtering. From that, by a simple path-length argument, the angular dependence of the yield was supposed to follow a $1/\eta=1/\cos q$ dependence. We will see later that there are substantial deviations from this result at all mass ratios except for $M_1 \ll M_2$. If the energy deposited in the first collision is assumed not to propagate away on a larger scale, one can insert the elastic *stopping power* $S_n(E)$ of the ion for the deposited energy in Eqs. (51a) and (51b). This approximation is only justified in some limiting cases that will be discussed below, since recoiling atoms may have considerable ranges. However, the stopping power can enter in many ways into a yield formula, both by qualitative and quantitative arguments. Since $S_n(E)$ is known over a large energy range with reasonable accuracy,[20] one would expect that for a given ion-target combination, any yield formula of the form $S(E)=bS_n(E)$ can be fitted to experimental data by use of only one adjustable parameter b. Thus, the variation of the yield with ion mass and angle of incidence is a better criterion for the validity of a yield formula than the yield-versus-energy curve for a specific ion-target combination.

Onderdelinden[15] and Joyes[11] treated energy deposition as a two-or three-step process, respectively. This is probably justified, since energy has degraded considerably in the second or third generation of recoil atoms. However, the mathematical treatment for realistic cross sections[15] (Joyes[11] assumed hard-sphere scattering) is almost as complex as the treatment of *all* steps, which is based on the integral equation.[24] Despite this, we will use two-step arguments in some applications later.

Onderdelinden[15] also introduced a characteristic depth x_0; the energy deposited within x_0 was assumed to be responsible for sputtering, so that, roughly, for an ion range R smaller than x_0, all energy is available for sputtering $[S(E)\alpha E]$, while for $R>x_0$, only the portion deposited within x_0 is of interest $[S(E)\alpha S_n(E)x_0]$. The depth x_0 was used as a fitting parameter. For Cu, $x_0=80$ Å, and for Au, $x_0=150$ Å. For Ar^+-Au bombardment, the energy of transition E_{12} between the linear and the nonlinear regime of the sputtering-yield curve is below 1 keV, according to experimental data.[1] Onderdelinden calculated $E_{12}\approx 4$ keV. Even at this energy, the average projected range[24,25] is only about 20 Å. The origin of the discrepancy between this value and the above 150 Å seems to be the basic assumptions underlying the fitting procedure. We will see at the end of the paper that the depth responsible for sputtering is nor constant, as assumed by Onderdelinden, but a certain fraction of the ion range, i.e., it increases with energy. The yield-versus-energy curve becomes linear at low energies because the stopping power is essentially linear [Eq. (33a) for $m=0$].

5. APPLICATIONS

This section deals with the application of the yield formulas (51a) and (51b) to various geometries of sputtering experiments. Emphasis will be laid on possible experimental arrangements to give independent measurements of the two major components of Eq. (51a): the deposited energy distribution $F(x,E,\eta)$ and the factors depending on target properties. This procedure has the effect that yield-versus-energy curves for backward sputtering by eV and keV ion beams will be discussed only at the end, although these measurements have been most frequent in experimental work.

The index (1) that distinguishes between the equal- and non-equal-mass cases will be dropped from now on, except in Sec. 5 C a iii.

A. Homogeneous Isotropic Sources

In this section we consider the sputtering by energetic particles from an isotropic source that is distributed homogeneously within a target.

Let us rewrite Eq. (51a) in the form

$$H(x,E,\eta)=\Lambda F(x,E,\eta), \tag{56a}$$

and let us forget, for the moment, that we have calculated the value of

$$\Lambda=\frac{3}{4\pi^2}\frac{1}{NC_0U_0}=\frac{0.0420}{NU_0\ \text{Å}^2} \tag{56b}$$

by use of a number of assumptions. According to the discussion in Sec. 4 F, Λ is a property of the target *material* and the state of the *surface*. In view of the uncertainties discussed there, accurate measurements of Λ would be desirable. It will turn out that homogeneous sources are the most suitable tool for this purpose.

We consider an infinite medium with a homogeneous isotropic source of recoiling atoms in the half-space $x\geq 0$ and an activity of Γ recoils per unit time and

volume. From Eqs. (22a) and (56a) we obtain the number of atoms sputtered into the half-space $x<0$ by a recoil at $y>0$:

$$S(x,E)=H_0(-x,E)=\Lambda F_0(-x,E)\,, \tag{57}$$

where F_0 is the zeroth coefficient of the Legendre polynomial expansion of $F(x,E,\eta)$. Let Φ be the total number of sputtered atoms per unit time and surface area. Then

$$\Phi=\Gamma\int_0^\infty S(x,E)dx=\Lambda\Gamma\int_0^\infty F_0(-x,E)dx. \tag{58}$$

Since F_0 is the depth distribution of deposited energy for an isotropic source, we have $F_0(-x,E)=F_0(x,E)$. Hence,

$$\int_0^\infty F_0(-x,E)dx=\frac{1}{2}\int_{-\infty}^\infty F_0(x,E)dx=\tfrac{1}{2}F_0^0(E)=\tfrac{1}{2}\nu(E)\,,$$

by use of Eq. (50b). This yields

$$\Phi=\tfrac{1}{2}\Lambda\Gamma\nu(E)\,. \tag{59a}$$

For a finite specimen with dimensions that are large compared to the radius of the collision cascades, one obtains the sputtering yield *S per primary particle*

$$S=\tfrac{1}{2}\Lambda(\Omega/W)\nu(E)\,, \tag{59b}$$

where Ω is the surface area and W the volume of the specimen. Equations (59a) and (59b) do not contain quantities that depend on the spatial distribution of the collision cascade and are independent of the macroscopic shape of the specimen. It should be possible to use Eq. (59a) or Eq. (59b) to determine both Λ and $\nu(E)$. Note that $\nu(E)\equiv E$ in the elastic collision region.

a. Radioactive Targets

Let us assume a silicon target doped homogeneously with Rn^{222} atoms at a concentration c (dopants/atom). The energy E_1 of the α particles is $E_1=5.5$ MeV, while the recoiling Po^{218} nuclei have $E_2\approx100$ keV. With the half-life τ, Eq. (59a) yields

$$\int_0^\tau\Phi(t)dt=\tfrac{1}{4}Nc\Lambda[\nu_1(E_1)+\nu_2(E_2)]\,, \tag{60}$$

where $\nu_1(E)$ and $\nu_2(E)$ apply to α particles and Po^{218} atoms, respectively. From Lindhard *et al.*,[40] we have $\nu_1(E_1)=12$ keV, while $\nu_2(E_2)$ is slightly smaller than E_2, around 90 keV. For a rough estimate, we insert Eq. (56b) for Λ. With a dopant concentration of 10^{-3}, one obtains about 10^{15} sputtered atoms/cm^2 within the half-life of $\tau=3.8$ days. (Concerning the surface binding condition of Si, see the discussion in Sec. 5 C.) The amount is large enough to be detected by tracer techniques. The significance of sputtering for the high volatility of α emitters has been pointed out by Riehl and Sizmann.[56] In their experiments, the activity was concentrated on the surface, so that only sputtering by the recoiling nuclei played a role. The present example shows that in homogeneously doped specimens the contribution from α particles is still small but not negligible.

b. Neutron Sputtering: Total Yield

The conditions underlying Eq. (59b) are satisfied if a target is immersed into an isotropic flux of fast neutrons in the core of a reactor. A neutron that hits the target creates $N\delta\sigma_n$ primary recoiling atoms in the average, where σ_n is the total neutron cross section and δ the average distance that a neutron travels through the target. Hence, the number of atoms sputtered from the whole surface is given by

$$S=2\Lambda gN\sigma_n\langle\nu(E)\rangle\,, \tag{61a}$$

where

$$g=\delta\Omega/4W \tag{61b}$$

is a geometric factor that is equal to unity for a spherical specimen, and $\langle\nu(E)\rangle$ is the average of $\nu(E)$ over the spectrum of recoil energies. For a spherical target, Eq. (61a) will also be applicable to beam experiments. For other targets the factor g depends on the orientation of the beam with respect to the target. For an order-of-magnitude estimate of the yield, we set $g=1$ for both in-pile and beam experiments.

The quantity $\langle\nu(E)\rangle$ has been calculated in connection with radiation damage studies.[57,58] For reactor irradiation, $\langle\nu(E)\rangle$ depends on the neutron spectrum. For gold, with the spectrum of the Munich reactor, Köhler and Schilling[57] calculated $\langle\nu(E)\rangle=4$ keV for both elastic and inelastic neutron scattering events.[59] The total cross section is ≈6 b in the energy region of interest. Inserting Eq. (56b) for a rough estimate of the yield, we obtain $S=1\times10^{-5}$ sputtered atoms per fast neutron (>0.1 MeV) for this particular reactor spectrum. For a pure fission spectrum, the expected yield is more than twice as high. For a 14-MeV neutron beam, one expects a value between 10^{-4} and 10^{-3} atoms per incident neutron.

Measurements have been done by several groups. Norcross *et al.*[60] report $S=(1.0^6\pm0.3)\times10^{-4}$ from in-pile measurements; Keller and Lee[61] got yields as high as $S\approx1$ with a Pu-Be source (≈4.2 MeV), a result that was withdrawn later. Keller,[62] with a minimum resolution of $S=6\times10^{-4}$, did not detect any sputtered atoms

[56] N. Riehl and R. Sizmann, Radiochim. Acta **1**, 44 (1964).
[57] W. Köhler and W. Schilling, Nukleonik **7**, 389 (1965).
[58] P. V. Thomsen (unpublished).
[59] In their evaluation, Köhler and Schilling (Ref. 57) did not make use of the Lindhard $\nu(E)$ function, but used a much less accurate expression. This inaccuracy, however, is insignificant in the case of gold, because the maximum recoil energy is well within the elastic collision region.
[60] D. W. Norcross, B. P. Fairand, and J. N. Anno, J. Appl. Phys. **37**, 621 (1966).
[61] K. Keller and R. V. Lee, J. Appl. Phys. **37**, 1890 (1966).
[62] K. Keller, Plasma Phys. **10**, 195 (1968).

when using a 14.1-MeV neutron beam, and Garber *et al.*[63] report $S=3\times10^{-3}$ on a single crystal, also with a 14.1-MeV beam. All data refer to gold, but scatter too much to allow a detailed comparison with experiment.

Equation (61a) also applies to thermal neutrons, when the cross section for (n,γ) processes is inserted for σ_n. The quantity $\langle\nu(E)\rangle$ can then be replaced by $\langle E\rangle$, since (n,γ) recoil energies are small (<1 keV). The relative importance of fast and thermal neutrons in sputtering is the same as in radiation damage, because both quantities are proportional to the factor $\sigma_n\langle\nu(E)\rangle$. The connection to radiation damage has already been pointed out by Taimuty.[64]

c. Fission Sources

In a target doped with fissioning nuclei, Eqs. (59a) and (59b) determine the number of ejected target atoms if $\nu(E)$ is replaced by $\langle\nu_1(E_1)+\nu_2(E_2)\rangle$, where the indices 1 and 2 distinguish between the two fission fragments, and the average is taken over the distribution of fragment masses. One can relate the sputtering yield to the number S_F of escaping fission fragments per unit time and volume. Fluegge and Zimen[65] determined the escape probability P for a particle with a well-defined range R to be $P=\frac{1}{4}(\Omega/W)R$. Hence, the ratio

$$\frac{S}{S_F}=2\Lambda\frac{\langle\nu_1(E_1)+\nu_2(E_2)\rangle}{\langle R_1(E_1)+R_2(E_2)\rangle} \tag{62}$$

gives the number of ejected atoms per escaping fission fragment. $R_1(E_1)$ and $R_2(E_2)$ are the ranges of the two fragments, range straggling being neglected. For uranium, Nilsson[66] reports an experimental value of $S/S_F=43$, while earlier measurements of Rogers and Adam[67] gave about 2000. The value of Nilsson[66] has to be corrected by a factor of $\frac{1}{2}$, since he assumed an escape rate of $P=\frac{1}{2}(\Omega/W)R$ in his data treatment instead of the above value. With a calculated[68] $\langle\nu_1(E_1)+\nu_2(E_2)\rangle=8.7$ MeV, a measured[69] $\langle R_1(E_1)+R_2(E_2)\rangle=19$ mg/cm², and Eq. (56b) for Λ ($U_0=5.56$ eV [70]), we obtain $S/S_F=28$. This agrees with Nilsson's corrected value of $S/S_F\approx22$ within experimental error.[66,71]

[63] R. I. Garber, G. P. Dolya, V. M. Kolyada, A. A. Modlin, and A. I. Fedorenko, Zh. Eksperim. i Teor. Fiz. Pis'ma v Redaktsiyu **7**, 375 (1968) [English transl.: Soviet Phys.—JETP Letters **7**, 296 (1968)].

[64] S. I. Taimuty, Nucl. Sci. Eng. **10**, 403 (1961).

[65] S. Fluegge and K. E. Zimen, Z. Physik Chem. **B42**, 179 (1939).

[66] G. Nilsson, J. Nucl. Mater. **20**, 231 (1966).

[67] M. D. Rogers and J. Adam, J. Nucl. Mater. **6**, 182 (1962).

[68] J. Lindhard and P. V. Thomsen, in *Symposium on Radiation Damage in Solids and Reactor Materials, Vienna, 1962*; *Radiation Damage in Solids I* (International Atomic Energy Agency, Vienna, 1962), p. 65.

[69] J. B. Niday, Phys. Rev. **121**, 1471 (1961).

[70] R. Hultgren, R. L. Orr, P. D. Anderson, and K. K. Kelley, *Selected Values of Thermodynamic Properties of Metals and Alloys* (John Wiley & Sons, Inc., New York, 1963).

[71] P. J. Peterson and M. M. Thorpe, Nucl. Sci. Eng. **29**, 425 (1967).

B. Deposited-Energy Function

While it is possible to calculate the deposited-energy function $F(x,E,\eta)$ in Eq. (56a) with much better accuracy than the material constant Λ, direct measurements of the dependence on x, E, and η would be desirable. The most interesting of the three variables is the depth variable x, both from an experimental point of view, since it determines the depth distribution of radiation damage,[24,39] and from a theoretical point of view, since reconstruction of a function of x from a finite number of averages $\langle x^n\rangle$ is a problem that does not have a unique solution, even when the general behavior of $F(x,E,\eta)$ is fairly obvious from physical arguments.

Backward sputtering experiments only determine F at $x=0$, so this particular geometry can only be used to check the dependence of F on E and η. Depth distribution measurements of radiation damage determine $F(x,E,\eta)$, but one has to be cautious in interpreting the damage observed near the target surfaces, since strain fields near a surface may impose conditions on the stability and annealing behavior of defects that are different from the bulk.

Sputtering experiments are therefore preferred in the present connection. In order to determine a depth dependence, one must move the source away from the surface, e.g., implanting radioactive atoms at a well-defined depth in the target, or move the surface away from the source, which can be realized in transmission sputtering experiments.

a. Edgeworth Expansion

In the elastic collision region, and at somewhat higher energies where electronic stopping is not dominating, the distribution $F(x)$ (we drop the variables E and η for the moment) is similar to a Gaussian, especially for $M_1\lesssim M_2$, where the ion undergoes a number of heavy deflection processes. Deviations from Gaussian shape are most pronounced when $M_1\gg M_2$, since in this case the ion trajectory is essentially a straight line with a rather well-defined length, so the deposited energy is determined primarily by the stopping power of the ion along the track. But in this case the recoiling atoms have considerable ranges, so there is still a good chance of getting a statistical distribution. This is different in the energy range where electronic stopping dominates and heavy elastic scattering events are infrequent. Then the function $F(x)$ is given by the variation of nuclear stopping with traveled path length, the latter quantity being governed by electronic stopping.

When $F(x)$ is similar to a Gaussian, one can approximate the function by the Edgeworth expansion[25,28,41,42]

in terms of the moments $\langle x^n\rangle$:

$$F(x)=\frac{\nu(E)}{\langle\Delta x^2\rangle^{1/2}}\left[\varphi_0(\xi)-\frac{\Gamma_1}{6}\varphi_3(\xi)+\left(\frac{\Gamma_2}{24}\varphi_4(\xi)+\frac{\Gamma_1^2}{72}\varphi_6(\xi)\right)+\cdots\right], \quad (63a)$$

where

$$\langle\Delta x^n\rangle=\langle(x-\langle x\rangle)^n\rangle, \qquad n=2,3,\cdots \quad (63b)$$

$$\varphi_n(\xi)=(d^n/d\xi^n)(2\pi)^{-1/2}e^{-\xi^2/2}, \quad n=0,1,2,\cdots \quad (63c)$$

$$\xi=(x-\langle x\rangle)/\langle\Delta x^2\rangle^{1/2}, \quad (63d)$$

$$\Gamma_1=\langle\Delta x^3\rangle/\langle\Delta x^2\rangle^{3/2}, \quad (63e)$$

$$\Gamma_2=\langle\Delta x^4\rangle/\langle\Delta x^2\rangle^2-3. \quad (63f)$$

If only the first term in the large square brackets is taken into account, one has a simple Gaussian with the width $\langle\Delta x^2\rangle^{1/2}$, centered around $x=\langle x\rangle$. The second term introduces the "skewness," and the third one the "excess" of the distribution. Similar types of expansions, using either Gaussian or non-Gaussian basal functions, have been investigated recently.[39]

Figure 6 shows the normalized distribution functions

$$\tilde{g}(\xi)=\frac{\langle\Delta x^2\rangle^{1/2}}{\nu(E)}F(x), \quad \int_{-\infty}^{\infty}\tilde{g}(\xi)d\xi=1, \quad (64a)$$

calculated for perpendicular incidence ($\eta=1$) and elastic scattering with the power cross sections (24a) and (24b) for $m=\frac{1}{2}$, and three representative mass ratios.

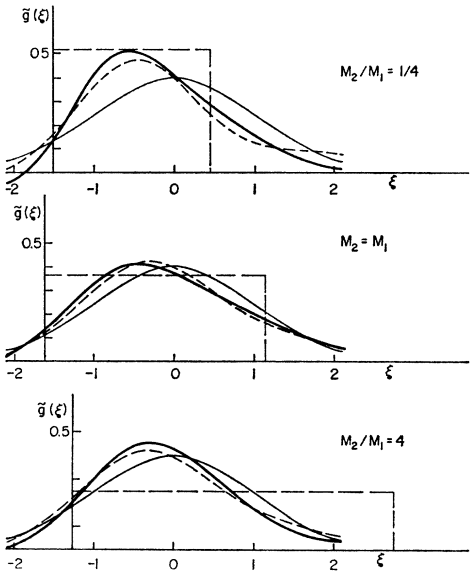

FIG. 6. Function $g(\xi)$ [Eq. (64)] for perpendicular incidence. $m=\frac{1}{2}$. Thin solid curve: Gaussian, first term in Eq. (63a); dashed curve: first and second term in Eq. (63a); thick solid curve: all three terms in Eq. (63a).

Input parameters $\langle\Delta x^n\rangle$ are taken from previous work.[24,28] The apparent over-all convergence of the expansion (63a) is good in all cases, but there is poor convergence in both tails of the distribution for $M_2/M_1=\frac{1}{4}$. The skewness is a sizable correction in all cases. The straight lines represent the stopping power as a function of traveled path length, under the assumption that the ion slows down along a straight line [for $m=\frac{1}{2}$ the stopping power does not depend on energy, according to Eqs. (33a) and (33b)]. These lines represent poor over-all approximations in all cases. Figure 7 shows a similar curve,

$$g(x)=\frac{1}{\nu(E)}F(x), \quad \int_{-\infty}^{\infty}g(x)dx=1, \quad (64b)$$

for a high-speed particle, where both electronic and nuclear stopping are inversely proportional to E, over the main part of the ion track. The figure is qualitative in every respect, the actual peak being much narrower, but it demonstrates clearly that a Gaussian is not a good zero-order approximation to $F(x)$ in this case.

Another important restriction on the validity of the Edgeworth expansion stems from the assumption of an infinite medium. Obviously, if a thin foil is bombarded whose thickness is smaller than the average penetration depth of the ion, the collision cascade cannot fully develop as in an infinite medium, and consequently less energy will be deposited in all depths. A general treatment of the effects of finite target thickness is beyond the scope of this paper. In the following we will assume either that target thickness is $\geq 2\langle\Delta x^2\rangle^{1/2}$, so that the main part of the Gaussian is inside the target, or that a target is so thin that the majority of the ions can penetrate with small energy loss.

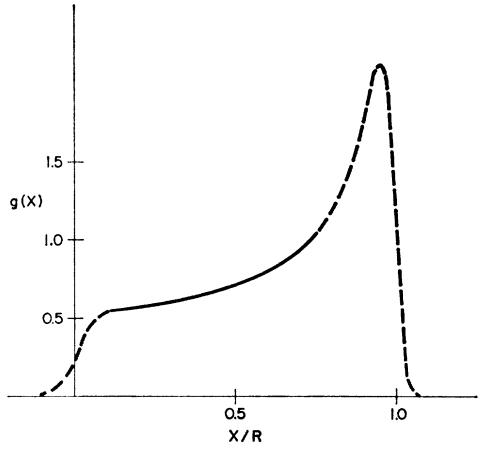

FIG. 7. Qualitative picture of the damage distribution in case of a high-speed particle with an initial energy in the Bethe-Bloch region. The dashed parts on both ends have been plotted on a magnified scale.

b. Angular Dependence of Moments

From Eqs. (50a) and (50b) one derives that only the moments F_0^0, F_1^1, F_0^2, F_1^3, F_3^3, etc., are different from zero. The angular dependence of the averages $\langle x^n\rangle$ can then be calculated from the relation

$$\int_{-\infty}^{\infty} x^n F(x)dx=\sum_{l=0}^{\infty}(2l+1)F_l^n P_l(\eta), \qquad (65a)$$

which follows from Eqs. (17), (20a), and (56a). The moments F_l^n are found from Eq. (50a). In order to simplify the interpretation of the distributions discussed in the following, we also introduce the averages over F for a point source. In this case, another coordinate system X, Y, Z is fixed to the beam, such that the source is in the origin and the beam is parallel to the X axis. The calculations in Refs. 22, 24, and 25 refer to this system of coordinates. One easily derives the following connections between the averages:

$$\langle x\rangle=\eta\langle X\rangle, \qquad (65b)$$

$$\langle x^2\rangle=\eta^2\langle X^2\rangle+(1-\eta^2)\langle Y^2\rangle, \qquad (65c)$$

$$\langle x^3\rangle=\eta^3\langle X^3\rangle+3\eta(1-\eta^2)\langle XY^2\rangle, \qquad (65d)$$

$$\langle x^4\rangle=\eta^4\langle X^4\rangle+6\eta^2(1-\eta^2)\langle X^2Y^2\rangle+(1-\eta^2)^2\langle Y^4\rangle. \qquad (65e)$$

Note that there is cylindrical symmetry around the X axis, i.e., $\langle Y^2\rangle=\langle Z^2\rangle$, etc.; Eqs. (65b)–(65e) do not involve any specific assumptions on the cross section. For elastic scattering with the power cross sections (24a) and (24b), the moments $\langle X^pY^{2q}\rangle$ have been calculated in Ref. 24 up to $n=p+2q=3$. Moments for $n=4$ are tabulated in Ref. 39.

For an isotropic source, one has to average over all η, so Eqs. (65b)–(65e) read

$$\langle x\rangle=0,\quad \langle x^2\rangle=\tfrac{1}{3}\langle R^2\rangle,\quad \langle x^3\rangle=0,\quad \langle x^4\rangle=\tfrac{1}{5}\langle R^4\rangle, \qquad (66a)$$

where

$$R^2=X^2+Y^2+Z^2. \qquad (66b)$$

c. Sputtering by Implanted Layers of Radioactive Atoms

If heavy radioactive ions are implanted into a light target, the depth distribution is relatively sharp, so measurements of the sputtering ratio as a function of the depth of the implanted layer determine the depth distribution of energy deposited by a plane isotropic source. Most feasible are α-active sources.[72] For the detection of long-range energy transport at low energies, Cd^+-implanted layers could be of interest, if activated by a source of thermal neutrons.

From Eqs. (57), (63a), and (66a) we obtain the sputtering yield per recoiling atom from a plane isotropic source at a distance x from the surface:

$$S(x,E)=\Lambda\left(\frac{3}{\langle R^2\rangle}\right)^{1/2}\nu(E)\left(\varphi_0(\xi)+\frac{\Gamma_2}{24}\varphi_4(\xi)\cdots\right), \qquad (67a)$$

where

$$\xi^2=\frac{3x^2}{\langle R^2\rangle},\quad \Gamma_2=3\left(\frac{3}{5}\frac{\langle R^4\rangle}{\langle R^2\rangle^2}-1\right). \qquad (67b)$$

The correction term $(\Gamma_2/24)\varphi_4(\xi)$ in Eq. (67a) determines the deviations from a Gaussian distribution and amounts to 10–20% of $\varphi_0(\xi)$, for $M_2/M_0\gtrsim\frac{1}{3}$ and $\xi\lesssim 2.5$ in the elastic collision region. For $M_2/M_1<\frac{1}{3}$ the correction is important $[\lesssim\frac{1}{2}\varphi_0(\xi)]$. From the measured dependence of $S(x,E)$ on x, one can obtain $\langle R^2\rangle$ for the particular recoil energy and, if the absolute value of $S(x,E)$ is measured, one can also determine Λ. In practice, $S(x,E)$ is folded with the range distribution of implanted ions, but this should not be an obstacle, especially for small range straggling ($M_1>M_2$). The sputtering by α particles only plays a role when the implanted depth is large compared to the range of recoil atoms.

One expects from Eq. (67a) that the sputtering yield should increase monotonically with decreasing implanted depth x. However, Eq. (67b) holds only when $x>(\frac{1}{3}\langle R^2\rangle)^{1/2}$; otherwise the surface is within the half-width of the distribution of deposited energy, which would cause Eq. (67a) to overestimate the sputtering yield.

Experimental results are not available to the author's knowledge. However, Riehl and Sizmann[56] measured the sputtering of an α-active *surface* layer evaporated on gold. Their reported sputtering yield, 57 ± 10 sputtered gold atoms for every recoil moving *into* the target, appears low when compared to the measured self-sputtering ratio of gold at *perpendicular* incidence, which is[73] $S\approx 52$. Nevertheless, it might be of interest to derive a modification of Eq. (67a) that would allow to calculate the sputtering of a radioactive surface layer.

Since only those recoils contribute to sputtering that move in the inward direction, we average Eq. (56a) only over the range $0\leq\eta\leq 1$. This yields

$$S(x,E)=\Lambda F(x,E),$$

with

$$F(x,E)=\sum_l(2l+1)a_l F_l(x,E),$$

where

$$a_l=\int_0^1 d\eta P_l(\eta).$$

Averages over $F(x,E)$ become, then,

$$\langle x\rangle=\tfrac{1}{2}\langle X\rangle,\quad \langle x^2\rangle=\tfrac{1}{3}\langle R^2\rangle,\quad \langle x^3\rangle=\tfrac{1}{4}\langle X^3\rangle+\tfrac{3}{4}\langle XY^2\rangle,$$

so

$$S(0,E)=\Lambda\frac{\nu(E)}{\langle\Delta x^2\rangle^{1/2}}\left[\varphi_0\left(\frac{-\langle X\rangle}{2\langle\Delta x^2\rangle^{1/2}}\right)\cdots\right], \qquad (68a)$$

where

$$\langle\Delta x^2\rangle=\tfrac{1}{3}\langle R^2\rangle-\tfrac{1}{4}\langle X\rangle^2. \qquad (68b)$$

[72] The significance of this experiment was pointed out to the author by J. A. Davis several years ago.

[73] O. Almén and G. Bruce, Nucl. Instr. Methods 11, 279 (1961).

Equation (68a) is not very reliable, since even for $M_1 > M_2$ the surface is always located within the half-width of the Gaussian, but the formula is certainly better than Eq. (67a) for $x=0$, since the surface does not coincide with the peak of the Gaussian. Because of the limited accuracy, there is no need for including higher terms of the Edgeworth expansion in Eq. (68a).

d. Transmission Sputtering: Low and Intermediate Ion Energies

We consider transmission sputtering of a foil of thickness d by a beam of ions of energy E, incident at an angle θ, where $\cos\theta=\eta$. The energy E should not be far up in the inelastic collision region, so that the distribution of deposited energy is not too different from a Gaussian. Then from Eqs. (56a) and (63a),

$$S(E,\eta)=\Lambda\frac{\nu(E)}{\langle\Delta x^2\rangle^{1/2}}\varphi_0(\xi), \tag{69a}$$

where

$$\xi=(d-\langle x\rangle)/\langle\Delta x^2\rangle^{1/2}, \quad \langle x\rangle=\eta\langle X\rangle,$$
$$\langle\Delta x^2\rangle=\eta^2\langle\Delta X^2\rangle+(1-\eta^2)\langle Y^2\rangle. \tag{69b}$$

Figure 8 shows calculated yields for transmission sputtering on gold foils of three different thicknesses bombarded by argon ions at perpendicular incidence, as a function of ion energy. The solid portions of the curves were calculated from Eq. (69a). Electronic stopping was taken into account semiquantitatively, by scaling all lengths with the $\rho(\epsilon)$ curve of Lindhard *et al.*[20] and calculating $\nu(E)$ from an analytic formula given in Ref. 40. Inelasticity plays a significant role, especially in the yield curve for $d=1000$ Å. At high energies, where $\langle x\rangle \gg d$, the majority of the argon ions penetrate the foil with little energy loss. The transmission sputtering yield can then be estimated roughly by use of Eqs. (70b) and (90). As it happens, the high-energy portions of the yield curves coincide with the backward yield on a thick target that is also included in Fig. 8. This is specific for the mass ratio $M_2/M_1=5$ of Ar^+-Au. When $M_2/M_1<5$, the backward sputtering yield is expected to be smaller than the high-energy portion of the transmission sputtering yield. The intermediate (dashed) parts of the curves are based on plausible interpolation between the low- and high-energy parts, taking into account that they must lie *below* the values predicted by Eq. (69a).

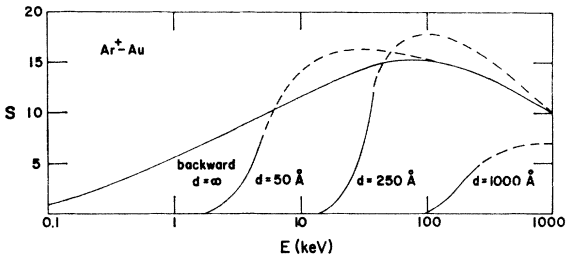

FIG. 8. Transmission sputtering yields calculated for Ar^+ ions incident on gold foils of three different thicknesses: $d=50$, 250, 1000 Å, as compared with the calculated yield for backward sputtering. For details see text.

Measurements at intermediate energies have been performed by Robinson[74] with molecular ions of hydrogen and deuterium incident on polycrystalline gold foils. The energy per incident *atom* varied between 5 and 15 keV, and the foil thickness between 500 and 1500 Å. Sputtering yields up to 0.025 per incident atom were recorded (maximum yield per molecule=0.0743). There are not enough data points at any fixed energy or foil thickness that would allow evaluation of $\langle x\rangle$ and $\langle\Delta x^2\rangle$, but the data can be compared to theory if one assumes $\langle x\rangle$ and $\langle\Delta x^2\rangle$ to be similar to the corresponding averages over the range distribution, the latter ones being known.[75] The similarity of range and damage distribution for $M_1 \ll M_2$ has been demonstrated for elastic collisions.[24] The magnitude of the measured yields turns out to be smaller by more than a factor of 10 than the yields calculated by use of Eq. (56b). From a comparison with measured *backward* sputtering yields of protons and deuterons incident on copper and silver,[76–78] it appears most likely that the main part of the discrepancy is due to an experimental error.

e. Transmission Sputtering: High Ion Energies

At high energies, the deposited energy is not distributed as a Gaussian. If the *emerging ion* has an energy E that is still high up in the inelastic collision region—which will usually be the case for MeV protons, α particles, and fission fragments penetrating foils—the deposited energy is primarily given by the elastic stopping power. However, recoil atoms may still lose energy to electrons, so the correct form of Eq. (56a) will be

$$S(E_1)=\alpha'\Lambda N\int_0^{\gamma E_1} d\sigma(E_1,T)\nu(T) \tag{70a}$$

if the ion escapes perpendicular to the surface. The factor α' ($\approx\frac{1}{2}$ for Rutherford scattering) takes into account the fact that some of the energy is not deposited inside the target surface. This will be discussed in detail in Sec. 5 C. When the relative energy loss of the ions in the foil is appreciable, Eq. (70a) may have to be averaged over the distribution of exit energies E_1, which can either be measured or calculated. Averaging over exit *angles* is only necessary in extreme cases. A $\cos^{-1}$ dependence will be reasonable for the latter purpose.

[74] C. H. Robinson, J. Appl. Phys. **39**, 3441 (1968).
[75] H. E. Schiøtt, Kgl. Danske Videnskab. Selskab, Mat.-Fys. Medd. **35**, No. 9 (1966).
[76] F. Grønlund and W. J. Moore, J. Chem. Phys. **32**, 1540 (1960).
[77] V. M. Gusev, M. I. Guseva, V. P. Vlasenko, and N. P. Elistratov, Izv. Akad. Nauk SSSR Ser. Fiz. **24**, 689 (1960) [English transl.: Bull. Acad. Sci. USSR Phys. Ser. **24**, 696 (1960)].
[78] O. C. Yonts, C. E. Normand, and D. E. Harrison, J. Appl. Phys. **31**, 447 (1960).

In the case where recoiling atoms have energies within the elastic collision region (e.g., 1-MeV protons incident on gold foils), Eq. (70a) reduces to

$$S(E_1)=\alpha' \Lambda N S_n(E_1). \tag{70b}$$

A yield measurement with this geometry has been made by Nelson and Thompson[79] with protons of initial energy 3.4 MeV bombarding a gold foil with preferred orientation. Under the conditions of this experiment, channeling of the protons can be excluded safely as a possible disturbing effect. The energy distribution of the emerging protons was rather broad, and centered around $E_1=300$ keV. At this energy, Eq. (70b) predicts a sputtering yield of 0.0025 atoms/ion. Nelson and Thompson measured 0.0007 for each of the three ⟨110⟩ spots in a {111} surface. This gives 0.0021 as the contribution of the spots to the total yield. The average yield is expected to be larger than 0.0025, since the energy distribution of the protons extends down to zero energy[79] and the sputtering yield increases as $1/E_1$ until E_1 comes down to about 10 keV. A more detailed comparison is not possible, since neither the energy distribution of emerging protons nor the total sputtering yield was measured.

This experiment played a unique role in the development of the field of sputtering, since a measurement of the *yield* was used to determine ranges of focused collision sequences. Obviously it is not necessary to invoke such long focusons (350 Å) in order to explain the measured sputtering yield.

f. Transmission Sputtering: Beams of Fast Neutrons

This case is very similar to the previous one. Usually the neutron beam will penetrate without appreciable scattering, so Eq. (70a) reads

$$S(E_n)=\Lambda N \sigma(E_n)\langle \nu(E)\rangle, \tag{71}$$

for perpendicular incidence, where $\sigma(E_n)$ is the total cross section of a neutron with energy E_n, and $\langle \nu(E)\rangle$ is the average of $\nu(E)$ over the spectrum of recoil energies. The factor α' in Eq. (70a) is very close to unity for fast neutrons. Of course, Eq. (71) differs from Eq. (61a) only by a geometric factor. Note that Eq. (71) determines the sputtering yield from the far side of the foil, while Eq. (61a) determines the total yield.

C. Backward Sputtering

Most experimental data on sputtering deal with backsputtering by ion beams. For this geometry, there exist experimental results that have been reproduced by different groups within an accuracy of typically 10–30%. Apart from various experimental conditions that influence the surface contamination,[1] a major factor limiting the accuracy of experimental data is the texture of polycrystalline targets.[80]

a. Elastic Collision Region

In the elastic collision region we have $\nu(E)=E$, so Eqs. (56a) and (63b) can be combined to give

$$S(E,\eta)=(\Lambda E/\langle \Delta x^2\rangle^{1/2})[\varphi_0(\xi_0)-\tfrac{1}{6}\Gamma_1\varphi_3(\xi_0)-\cdots], \tag{72a}$$

where

$$\xi_0=-\langle x\rangle/\langle \Delta x^2\rangle^{1/2}. \tag{72b}$$

For the power cross section (24a), the moments $\langle x^n\rangle$ have the general form[24,39]

$$\langle x^n\rangle=(E^{2m}/NC)^n h_n(\eta), \tag{73}$$

where $h_n(\eta)$ is some function of η. This means that ξ_0, and therefore the contents of the brackets in Eq. (72a), is independent of ion energy. The factor in front of Eq. (72a) is proportional to NCE^{1-2m}, which is essentially the stopping power. Hence, the sputtering yield is a product of the stopping power of the ion and some function of the angle of incidence. The latter function may depend on m and the mass ratio M_2/M_1.

i. Variation with angle of incidence: moderate-mass ratios. In order to estimate the dependence of $S(E,\eta)$ on η, we only take into account the term $\varphi_0(\xi_0)$ in the brackets of Eq. (72a). Figure 6 indicates that neglecting the φ^3 term may not be justified for $M_1 \gg M_2$. Note that decreasing η means a shift of the distribution $\tilde{g}(\xi)$ toward the surface, apart from a change in the shape of the distribution.

Inserting Eqs. (65b) and (65c) into Eqs. (72a) and (72b), we obtain the variation of the yield with η,

$$\frac{S(E,\eta)}{S(E,1)}=\left(\eta^2+(1-\eta^2)\frac{\langle Y^2\rangle}{\langle \Delta X^2\rangle}\right)^{-1/2} \times\exp\left[\frac{\langle X\rangle^2}{2\langle \Delta X^2\rangle}\left(1+\frac{\eta^2}{1-\eta^2}\frac{\langle \Delta X^2\rangle}{\langle Y^2\rangle}\right)^{-1}\right], \tag{74}$$

where $S(E,1)$ is the yield for perpendicular incidence. With the moments $\langle X\rangle$, $\langle \Delta X^2\rangle$, and $\langle Y^2\rangle$ that are tabulated in Ref. 24, Eq. (74) can be evaluated, and $S(E,\eta)$ turns out to increase monotonically with decreasing η.

For not-too-oblique incidence, one can approximate Eq. (74) by

$$\frac{S(E,\eta)}{S(E,1)}=\eta^{-f}=(\cos\theta)^{-f}, \quad \eta\approx 1 \tag{75a}$$

where the exponent f is found by expanding Eq. (74) in powers of $1-\eta^2$. We obtain

$$f=1+\frac{\langle Y^2\rangle}{\langle \Delta X^2\rangle}\left(\frac{\langle X\rangle^2}{\langle \Delta X^2\rangle}-1\right). \tag{75b}$$

[79] R. S. Nelson and M. W. Thompson, Proc. Roy. Soc. (London) **259**, 458 (1961).

[80] A. L. Southern, W. R. Willis, and M. T. Robinson, J. Appl. Phys. **34**, 153 (1963).

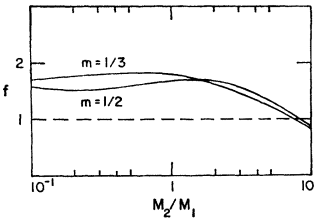

FIG. 9. Factor f determining the dependence of sputtering ratio on angle of incidence as defined in Eqs. (75a) and (75b).

Figure 9 shows f as a function of mass ratio, for $m=\frac{1}{2}$ and $m=\frac{1}{3}$. The two curves essentially agree, so the angular variation of the yield will not be sensitive to ion energy, and for $M_2/M_1 \lesssim 3$ the exponent f is about $\frac{5}{3}$, independent of the mass ratio. Both conclusions are in complete agreement with recent experimental results.[81]

For grazing incidence, Eq. (74) predicts

$$\frac{S(E,0)}{S(E,1)}=\left(\frac{\langle \Delta X^2\rangle}{\langle Y^2\rangle}\right)^{1/2}\exp\left(\frac{\langle X\rangle^2}{2\langle \Delta X^2\rangle}\right). \tag{76}$$

We know from experiment[82,83] that the sputtering yield goes through a maximum at very oblique incidence and approaches zero for $\theta=90°$. This maximum cannot be explained on the basis of the assumption of an infinite medium. There will be a certain glancing angle at which the repulsive action of the surface atoms is strong enough to prevent the ions from penetrating into the target, and this angle will, in general, depend on the structure of the surface as indicated by experiment.[83] If we only consider nongrazing incidence, Eq. (76) gives an indication of the range of validity of the expansion (75a). Figure 10 shows that the ratio $S(0)/S(1)$ depends on the mass ratio but is insensitive to m, i.e., the ion energy. In the region $M_2/M_1 \lesssim \frac{1}{3}$ (dashed curves in Fig. 10) the Guassian approximation is expected to fail. The value of $S(0)/S(1)$ should agree at least qualitatively with the observed ratio $S(\eta_{max})/S(1)$ in the maximum. Ratios of 4–5 have been measured by Cheney and Pitkin[83] with both Xe^+ and Ar^+ ions incident on copper targets, in good agreement with Fig. 10. Figure 11 shows the variation of the Ar^+-Cu sputtering ratio with angle of incidence as compared to experimental results of several groups. The agreement is very satisfactory for $\theta \lesssim 70°$. The experimental data of four different groups,[81,83–85] together with the theoretical prediction of Eq. (74), clearly show that the $1/\cos\theta$ dependence that was measured,[82] calculated,[5,7–10] or postulated[15] previously, is too weak for $\theta \lesssim 70°$. Only for $M_1 \ll M_2$ is the $1/\cos\theta$ dependence appropriate, according to Fig. 9.

ii. Variation with ion mass. We concluded in the beginning of Sec. 5 C a that the energy dependence of the sputtering yield is determined by the stopping power. For perpendicular incidence, we write

$$S(E)=\Lambda\alpha N S_n(E), \tag{77}$$

where $S_n(E)=[1/(1-m)]C\gamma^{1-m}E^{1-2m}$ is the eleastic stopping power of the ion [Eq. (33b)], and α is a factor that depends only on m and M_2/M_1. The accuracy of

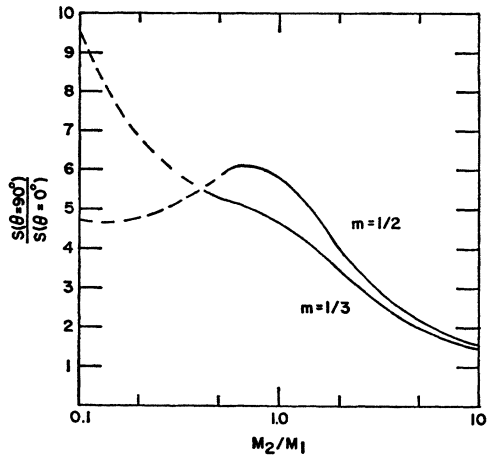

FIG. 10. Calculated ratio of the sputtering yields for grazing and perpendicular incidence, from Eqs. (76). The repulsive action of the surface on the incident ion has been neglected.

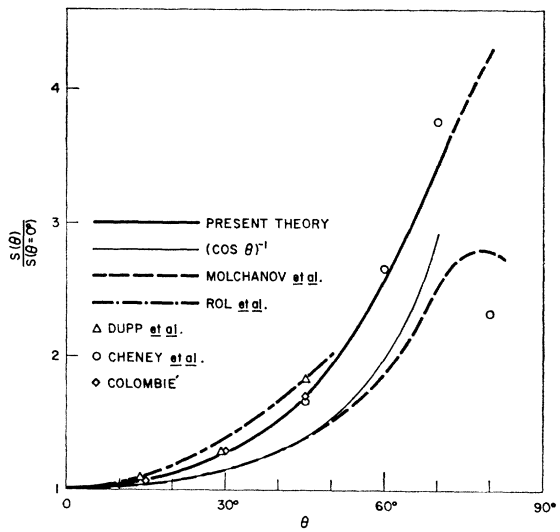

FIG. 11. Variation of the sputtering yield with angle of incidence for Ar^+ ions incident on polycrystalline copper. Thick solid curve: Eq. (74) evaluated for $m=\frac{1}{2}$; thin solid curve: $1/\cos\theta$. Experimental results of Dupp and Scharmann (Ref. 81), Molchanov and Tel'kovskii (Ref. 82), Cheney and Pitkin (Ref. 83), Rol *et al.* (Ref. 84), and Colombié (Ref. 85).

[81] G. Dupp and A. Scharmann, Z. Physik **194**, 448 (1966).
[82] V. A. Molchanov and V. G. Tel'kovskii, Dokl. Akad. Nauk SSSR **136**, 801 (1961) [English transl.: Soviet Phys.—Doklady **6**, 137 (1961)].
[83] K. B. Cheney and E. T. Pitkin, J. Appl. Phys. **36**, 3542 (1965).
[84] P. K. Rol, J. M. Fluit, and J. Kistemaker, Physica **26**, 1000 (1960).
[85] N. Colombié, thesis, University of Toulouse, 1964 (unpublished).

the calculated value of α depends on how accurately the deposited energy function is approximated by a finite number of terms in the Edgeworth expansion. Figure 12 shows α as a function of M_2/M_1 for $m=\frac{1}{2}$ and $m=\frac{1}{3}$. The curves labaled "Gaussian" follow from neglecting everything except the Gaussian in the brackets of Eq. (72a), and the curves labeled "corrected Gaussian" take into account the term proportional to $\varphi_3(\xi_0)$. The third set of curves, called "non-Gaussian," also stems from an expansion of the type of Eq. (72a), but with a basal function $\varphi_0(\xi)=\text{const}\times\exp(-\lambda|\xi|^\beta)$, where β is different from 2, and chosen to give the correct ratio $\langle\Delta X^4\rangle/\langle\Delta X^2\rangle^2$. Details of this expansion have been discussed elsewhere.[39] Comparison of Fig. 12(a) with Fig. 12(b) shows that the two sets of curves are very similar, and that the three approximations give nearly the same results except for $m=\frac{1}{2}$, $M_2/M_1<\frac{1}{2}$. The horizontal lines labeled "limit $M_1\gg M_2$" are based on the assumption that the ion is not deflected while penetrating the layer that is relevant for sputtering. The derivation follows in the next subsection. These lines are supposed to represent the case $M_1\gg M_2$ rather accurately.

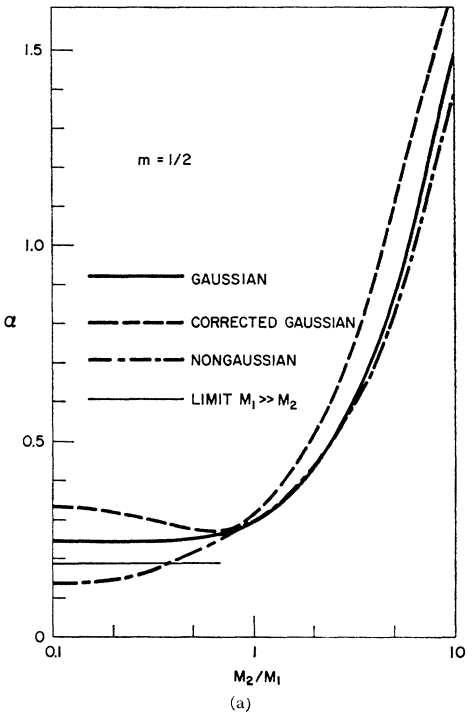

FIG. 12. Factor α [Eq. (77)] as a function of mass ratio for four different approximations to the distribution function of deposited energy. (a) $m=\frac{1}{2}$; (b) $m=\frac{1}{3}$.

It appears most reasonable for further evaluation to use the Gaussian approximation for $M_1\lesssim M_2$, since it appears to compromise between the other two approximations, and the asymptotic straight lines for $M_1\gg M_2$. If we remember the limited accuracy of the power cross sections, the difference between Figs. 12(a) and 12(b) does not appear significant enough to justify the use of two different curves of α versus M_2/M_1 for $m=\frac{1}{2}$ and $m=\frac{1}{3}$. We therefore take the arithmetic means of both the Gaussians and the asymptotic straight lines (Fig. 13) and make a reasonable interpolation in the range $0.2\lesssim M_2/M_1\lesssim 0.5$. The accuracy of the resultant curve α versus M_2/M_1 is estimated to be 10–20% within the elastic collision region. It has been checked that the curve α versus M_2/M_1 for $m=\frac{1}{4}$,

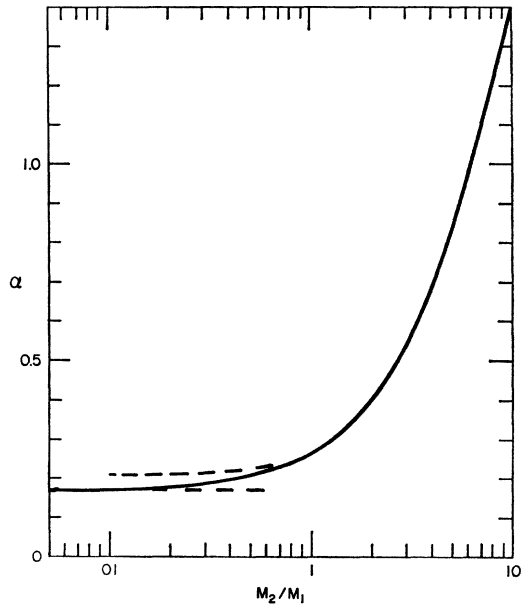

FIG. 13. Factor α [Eq. (77)] as a function of mass ratio in the elastic collision region.

which is of interest in low-energy sputtering, agrees closely (better than 10%) with the one for $m=\frac{1}{3}$ [Fig. 12(a)] at all mass ratios. The same is true for $m=\frac{2}{3}$ and $m=\frac{1}{2}$, but the uncertainty at small mass ratios is even larger for $m=\frac{2}{3}$ than in Fig. 12(a) for $m=\frac{1}{2}$. Once α has been found independent of m, one recognizes that $S_n(E)$ is the only quantity entering Eq. (77) that depends on the ion-target interaction cross section. It is therefore appropriate to use the best approximation for $S_n(E)$ that is available and *not* the power cross sections for the purpose of comparison with experiment. We will use the Thomas-Fermi cross section as calculated by Lindhard *et al.*[20] at sufficiently high energies [$>E^*_1$ Eq. (34)] and the expression

$$S_n(E)=C_0T_m=\tfrac{1}{2}\pi\lambda_0a^2T_m \tag{78}$$

at lower energies. Equation (78) follows from Eq. (33b) by setting $m=0$ and inserting Eq. (28′). A comparison with experimental results is postponed to Sec. 5 C c.

iii. The case $M_1\gg M_2$. It is obvious from Fig. 12(a) —and was concluded before[28]—that the Edgeworth expansion does not converge rapidly for small mass ratio M_2/M_1. In order to determine the factor α in this case with some accuracy, we calculate the deposited energy in an alternative way that is appropriate whenever the ion penetrates the significant layer for sputtering essentially undeflected, and with only small relative energy loss. We consider perpendicular incidence first. The deposited energy at the surface $x=0$ becomes, then,

$$F_{(1)}(0,E,1)$$
$$=N\int_0^\infty dx\int_0^{T_m}d\sigma_{(1)}(E,T)F(-x,T,\cos\varphi'')\,, \tag{79}$$

where $F(-x,T,\cos\varphi'')$ is the deposited energy function for an atom recoiling at a distance x from the surface with energy T and an angle φ'' [$\cos\varphi''=(T/T_m)^{1/2}$] to the surface normal, and $Ndxd\sigma_{(1)}(E,T)$ is the probability for the ion to create such a recoil atom while traveling through dx. We introduced the index (1) again in order to distinguish between ion and recoil atom. The intergation over dx has been extended to infinity, since F falls off rapidly as a function of x (Fig. 6). The dependence of E on x in $d\sigma_{(1)}(E,T)$ has been ignored, because of the assumption of small average energy loss in the relevant layer, and deflection of the ion has been neglected. Interchanging the order of integrations, we can rewrite Eq. (79) as

$$F_{(1)}(0,E,1)=N\int_0^{T_m}d\sigma_{(1)}(E,T)T\gamma(\cos\varphi'')\,, \tag{80a}$$

where we made use of the definition[28]

$$\gamma(\eta)=\frac{1}{E}\int_{-\infty}^{0}dxF(x,E,\eta)\,. \tag{80b}$$

γ was called the sputtering efficiency, and turned out to be independent of ion energy for a given power cross section. Apart from this exact result, γ is also insensitive to m.[28] The variation of γ with the directional cosine η is strong. For perpendicular incidence, γ is typically a few percent, while it becomes $\frac{1}{2}$ for $\eta=0$ in an infinite medium.

Numerical calculations show that $\gamma(\eta)$ is approximately a parabola.[86] We evaluate the integral equation (80a) by assuming two different parabolas for $\gamma(\eta)$:

$$\gamma_1(\eta)=\tfrac{1}{2}(1-\eta)^2\,, \tag{81a}$$

$$\gamma_2(\eta)=\gamma_p+(\tfrac{1}{2}-\gamma_p)(1-\eta)^2\,, \tag{81b}$$

where γ_p is the value of γ for perpendicular incidence. The experimental result is[29] $\gamma_p\approx0.028$ for $M_1=M_2$. Equation (81b) should be a better approximation than Eq. (81a), since it has the correct values at both $\eta=1$ and $\eta=0$. By evaluating the integral with the cross section (24b) and taking into account the definition of α [Eq. (77)], we obtain

$$\alpha=\alpha_1=[2(3-2m)(2-m)]^{-1} \tag{82a}$$

from Eq. (81a), or

$$\alpha=\alpha_2=\alpha_1+\Delta\alpha\,,\quad \Delta\alpha=\gamma_p\frac{(1-m)(5-2m)}{(3-2m)(2-m)} \tag{82b}$$

from Eq. (81b). Note that m characterizes the *ion*. With $\gamma_p=0.028$ we get $\alpha_1=0.167$ and $\alpha_2=0.186$ for $m=\frac{1}{2}$, and $\alpha_1=0.129$ and $\alpha_2=0.150$ for $m=\frac{1}{3}$. The straight lines $\alpha=\alpha_2$ have been drawn up in Figs. 12(a) and 12(b) with the label "limit $M_1\gg M_2$."

Note that the integrand in Eq. (80a) is a *monotonically decreasing* function of T, so it must be predominantly the *soft* collisions that contribute to sputtering. Moreover, the relative contribution of soft collisions to the total sputtering yield is greater than their contribution to the stopping power. This is a very important result. Note that it was derived under the two assumptions of perpendicular incidence and no deflection.

For oblique incidence the procedure is very similar. Taking over the notations of Sec. 2, we evaluate the expression

$$F_{(1)}(0,E,\eta)=N\int_0^\infty dx\int d\sigma_{(1)}(\mathbf{v},\mathbf{v}'')F(-x,T,\eta'')$$
$$=N\int d\sigma_{(1)}(\mathbf{v},\mathbf{v}'')T\gamma(\eta'')\,, \tag{83}$$

where η'' is the directional cosine of a recoiling atom to the surface normal. We insert the cross section (24b) and replace the energy variable T by the angular variable $\cos\varphi''$ and the azimuthe χ'' of the recoil

[86] K. B. Winterbon (unpublished).

direction:

$$F_{(1)}(0,E,\eta)=2NC_{(1)}E^{-m}T_m^{1-m}\times\int_0^1 d\cos\varphi''\int_0^{2\pi}\frac{d\chi''}{2\pi}(\cos\varphi'')^{1-2m}\gamma(\eta''),$$

or, with the definition of α [Eq. (77)] and the stopping power from Eq. (44b),

$$\alpha=2(1-m)\int_0^1 d\cos\varphi''\times(\cos\varphi'')^{1-2m}\int_0^{2\pi}\frac{d\chi''}{2\pi}\gamma(\eta''), \quad (84a)$$

where

$$\eta''=\cos\theta\cos\varphi''+\sin\theta\sin\varphi''\cos\chi'' \quad (84b)$$

and θ the angle of incidence with respect to the surface normal.

For oblique incidence, the directional cosine η'' in Eq. (84b) can take on negative values. The expressions $\gamma_1(\eta)$ and $\gamma_2(\eta)$ in Eqs. (81a) and (81b), however, only hold for positive values of η.

From the obvious relation

$$F(x,E,-\eta)=F(-x,E,\eta)$$

that holds for an infinite medium, we derive by use of the definition (80b) and the normalization (50c) that

$$\gamma(\eta)=1-\gamma(-\eta). \quad (85)$$

Equation (85) is used to define $\gamma(\eta)$ for negative values of η. The two integrations in Eq. (84a) can then be performed. The calculation is cumbersome but straightforward. We are mainly interested in the result for nearly perpendicular incidence, where $1-\eta^2=\sin^2\theta$ is small. Writing down the terms of lowest order in $\sin^2\theta$, we obtain

$$\alpha=\alpha_2+(1-2\gamma_p)\frac{5-4m}{4(3-2m)(2-m)}\times\sin^2\theta-(1-2\gamma_p)\frac{1}{4\pi}\frac{B(\frac{1}{2},\frac{3}{2}-m)}{(2-m)^2}(\sin^2\theta)^{2-m}\cdots, \quad (86)$$

where α_2 is defined in Eq. (82b) and $B(\frac{1}{2},3-m)$ is a β function as defined in Eq. (42a). Equation (86) holds for $m<1$.

By use of Eq. (82b), we can also write

$$\frac{S(\eta)}{S(1)}=\frac{\alpha}{\alpha_2}=1+\frac{(1-2\gamma_p)(5-4m)}{1+2\gamma_p(1-m)(5-2m)}\frac{\sin^2\theta}{2}-\frac{(1-2\gamma_p)B(\frac{1}{2},\frac{5}{2}-m)}{1+2\gamma_p(1-m)(5-2m)}\frac{(\sin^2\theta)^{2-m}}{\pi}\cdots, \quad (87a)$$

which, by means of Eq. (75a), gives

$$f=\frac{(1-2\gamma_p)(5-4m)}{1+2\gamma_p(1-m)(5-2m)}, \quad (87b)$$

provided that the term of order $2-m$ can be neglected. With $\gamma_p=0.028$, we obtain $f=2.54$ for $m=\frac{1}{2}$ and $f=2.98$ for $m=\frac{1}{3}$, indicating the the angular dependence is somewhat more pronounced for small θ than indicated by Fig. 9, for $M_2/M_1\ll 1$. However, the term with $(\sin^2\theta)^{2-m}$ is appreciable especially for $m=\frac{1}{2}$. Figure 14 shows a comparison with experimental results by Holmén and Almen[87] for graphite bombarded with mercury ions. The agreement between Eq. (87a) and the experimental results is very satisfactory for $\theta\lesssim 45°$.

b. High and Intermediate Energies

The effect of electronic stopping on the sputtering-yield formula cannot be described in full detail at present, since the numerical solutions of Eq. (50a), including inelasticity, are not available yet. As in previous sections, however, a number of cases can be treated without detailed knowledge of the deposited-energy function, and some examples will be considered here.

i. Ions in the Rutherford region. At high enough energies, even very light ions have a vanishingly small probability of undergoing heavy deflections near the surface. Hence, the considerations of the foregoing section concerning the case $M_1\gg M_2$ should also be applicable here. Let us first consider the case where the majority of the *recoiling* atoms have energies in the elastic collision region (e.g., 1-MeV protons bombarding gold). Then Eq. (77) should determine the sputtering yield with α given by Eqs. (82a) and (82b) for $m=1$ (Rutherford scattering). We get $\alpha=\alpha_1=\alpha_2=\frac{1}{2}$. Figure 7 shows that because energy dissipation starts at $x=0$, some energy is deposited at $x<0$, so less energy will be deposited in the surface than would be calculated from the stopping power. We have $\alpha=\frac{1}{2}$ because most

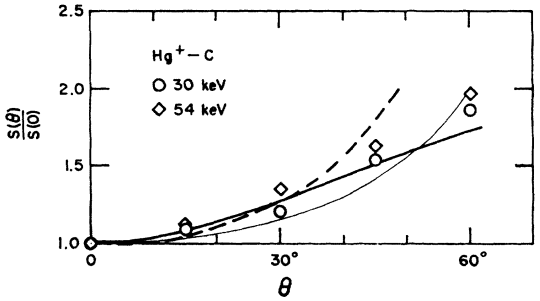

FIG. 14. Angular dependence of sputtering yield for Hg^+ ions incident on graphite. Experimental points from Holmén and Almén (Ref. 87). Thick solid curve: Eq. (87a) for $m=\frac{1}{2}$; dashed curve: $(\cos\theta)^{-f}$ with $f=5/3$ (Fig. 9); thin solid curve: $1/\cos\theta$.

[87] G. Holmén and O. Almén (to be published).

recoils move perpendiuclar to the beam, and $\gamma(\eta=0)=\frac{1}{2}$, according to Eqs. (81a) and (81b). If we had taken into account the existence of a real surface in the calculation of the deposited-energy function, α might have become slightly smaller.

Obviously, because low-energy recoils moving perpendicular to the beam dominate so heavily, it does not make any difference whether the proton *enters* or *leaves* a target with a certain energy E at a certain angle θ. Therefore, backsputtering and transmission sputtering are equivalent in the Rutherford collision region, except, of course, for the effects of energy loss and multiple scattering of an ion penetrating a foil with finite thickness. This is the reason why we have $\alpha'=\alpha=\frac{1}{2}$ in Eq. (70a).

The angular dependence of the sputtering yield follows from Eq. (87a). For $m=1$, both the second and the third terms are proportional to $\sin^2\theta$. However, for $m=1$, a fourth term must be taken into account that is equal to the third but with opposite sign. Therefore,

$$S(\theta)/S(0)=1+(1-2\gamma_p)\sin^2\theta\approx(\cos\theta)^{-0.94} \quad (88)$$

for Rutherford scattering and not-too-large θ. This result also holds for both backward and transmission sputtering.

If the ion energy is so high that recoil atoms lose a substantial part of their energy in electronic collisions, one has to replace the stopping power $S_n(E)$ in Eq. (77) by the integral

$$\int_0^{T_m} d\sigma(E,T)\nu(T)\,,$$

just as in Eq. (70a).

ii. Backsputtering by fast neutrons. The initial assumption made in Sec. 5 C a iii—that the bombarding particle penetrates a certain layer essentially undeflected and with negligible energy loss—is ideally fulfilled for fast neutrons. The cross section, however, does not have the form (24b). We note that the quantity α in Eqs. (82a) and (82b) is determined by the dependence of $d\sigma_{(1)}$ on T, while the dependence on E only enters the stopping power. Thus, assuming isotropic scattering as a rough approximation, we write

$$d\sigma_n=\sigma_n(E)dT/T_m \quad (89)$$

for the differential cross section of a fast neutron, and therefore we can apply the results of Sec. 5 C a iii with $m=-1$.

Equations (82a) and (82b) yield $\alpha_1=1/30$ and $\Delta\alpha=14\gamma_p/15$, so $\alpha=0.0595$, indicating that backsputtering by fast neutrons is a negligibly small effect, as far as *elastic* scattering of neutrons is concerned. This is because isotropic scattering causes most energy to travel toward the inner regions of the target.

We wish to compare the above result to the case of *transmission* sputtering. Equation (79) applies to this situation if the variable $-x$ is replaced by x. Then, making use of Eq. (85), we obtain

$$\alpha'=1-\alpha\,, \quad (90)$$

where α' is the quantity introduced in Eq. (70a). Since $\alpha\ll1$ for fast neutrons, we could set $\alpha'\approx1$ in Eq. (71). We conclude that about 17 times as much material is sputtered from the far side of the target as from the side where the beam hits, for perpendicular incidence when inelastic scattering can be neglected.

For light elements, electronic stopping of recoil atoms will become important. This affects the sputtering yield in two ways. First, as usual, we have to replace the recoil energy T by $\nu(T)$ in the stopping power. This reduces both backward and transmission sputtering. Second, the radius of the recoil cascades will be smaller. This will reduce α further, while α will not be affected. Thus, the ratio between backward and transmission sputtering yields may be even smaller than 1/17 when inelastic scattering of the neutrons is unimportant. A substantial difference between backward and transmission sputtering has been measured,[61] but because of the apparent uncertainties in the measured sputtering yields, a quantitative comparison is not yet possible.

For the angular dependence of the backsputtering yield, Eq. (87a) predicts, for $m=-1$,

$$S(\theta)/S(0)=1+4.76\times\tfrac{1}{2}\sin^2\theta\approx(\cos\theta)^{-4.76}. \quad (91)$$

This strong dependence on θ is not surprising in view of the small yield for perpendicular incidence.

Note that the results of this sub-section could also be applied to the earlier sputtering theories where the primary scattering cross section was assumed to be isotropic, and sputtering was assumed to be caused by the first collision undergone by the ion.[5,7,9] Comparison of the value $\alpha'=0.0595$ with Fig. 13 shows that the calculated sputtering yield would then be too small by about an order of magnitude.

iii. Ions in moderate inelastic collision region. This is the most complex case. Except for $M_1\gg M_2$, violent deflections of the ion must be taken into account, so electronic stopping of both the *ion* and the recoiling atoms influences the sputtering yield. Because of a decrease in penetration depth, the cascades develop closer to the surface, so the possibility cannot be ruled out that for special ion-target combinations over a certain energy range, electronic stopping may give rise to an *increase* in sputtering yield. Certainly there may be a partial cancellation of the three effects. We will assume elastic stopping in the following, but have to bear in mind that the error made may be substantial. This point is hoped to be improved in the near future, when Eqs. (50) have been solved numerically.

iv. Protons and deuterons at intermediate energies. If the α-versus-mass-ratio curves in Figs. 12 and 13 were continued to the abscissa of $M_2/M_1=197$ for protons bombarding gold, one would arrive at an enormous

sputtering yield. However, both protons and deuterons undergo predominantly electronic collisions at essentially all energies,[75] so that our derivation does not apply to the case. We show by a simple calculation that α is of the order of unity for protons and deuterons. From Eq. (63) and the definition of α [$F(x=0)=\alpha N S_n(E)$], we obtain

$$\alpha=\frac{1}{NS_n(E)}\frac{\nu(E)}{\langle\Delta x^2\rangle^{1/2}}(2\pi)^{-1/2}\exp\left(-\frac{\langle x\rangle^2}{2\langle\Delta x^2\rangle}\right), \quad (92)$$

taking into account only the Gaussian part of the distribution of deposited energy. For not-too-light targets, we can neglect electronic stopping of *recoil atoms*. Then we have[40]

$$\frac{d\nu(E)}{dE}=\frac{S_n(E)}{S_n(E)+S_e(E)}\approx\frac{S_n(E)}{S_e(E)}.$$

Inserting Eq. (23a) for $S_e(E)$ and assuming $S_n(E)=\text{const}$ ($m=\frac{1}{2}$), we get

$$\nu(E)=2ES_n/S_e. \quad (93)$$

Inserting this into Eq. (92) and going over to dimensionless energy and length units ϵ and ρ, respectively,[21,40] Eq. (92) reads

$$\alpha=\frac{\epsilon^{1/2}}{(\frac{1}{4}k^2\langle\Delta\rho^2\rangle)^{1/2}}(2\pi)^{-1/2}\exp\left(-\frac{1}{2}\frac{\langle\rho^2\rangle}{\langle\Delta\rho^2\rangle}\right), \quad (94)$$

where k is the electronic stopping constant in dimensionless units.[21,40] The quantities $\langle\rho\rangle$ and $\langle\Delta\rho^2\rangle$ could be calculated by use of Schiøtt's procedure.[75] For a rough estimate, it is sufficient to assume that the distribution of deposited energy coincides with the distribution of projected ranges.[24] The latter distribution is known from Schiøtt's work. Since the quantities $\frac{1}{4}k^2\langle\Delta\rho^2\rangle$ and $\langle\Delta\rho^2\rangle/\langle\rho\rangle^2$ do not depend on the target, α depends only on the ion and the energy. Figure 15 shows α as a function of ϵ for protons and deuterons. The accuracy of the curves is hardly better than the difference between the proton and deuteron curve, and neither curve should be used for the purpose of a quantitative comparison with experiment. It is obvious, however, that at intermediate energies ($\epsilon\approx1$), backscattering of ions causes α to be substantially greater than the high-energy value $\alpha=\frac{1}{2}$, but much smaller than the value that would result from assuming purely elastic scattering.

Note that for $\epsilon<1.5$ we have[75] $\langle\Delta\rho^2\rangle^{1/2}>\langle\rho\rangle$, which indicates that Fig. 15 overestimates α in this energy region because of the neglect of the surface in our calculation.

c. Comparison with Experimental Yield-versus-Energy Curves

Before calculating absolute yield curves, we have to make a decision concerning the surface binding conditions. Equations (48a) and (48b) express two kinds of uncertainties: first, the question of whether the ejection probability is approximately isotropic or follows a work-function model; second, the relative significance of the bulk and surface binding energies V and U_0, respectively. At present we solve the problem by definition, but note that analysis of energy and angular distributions (Paper II) may give additional information:

(a) For metals, we use the work-function model (35) with $V=0$ and U_0 equal to the measured sublimation energy.

(b) For covalent crystals, we assume an isotropic ejection probability [Eq. (36)] with U_0 equal to the measured cohesive energy per atom, and V twice this value.

Assumption (b) has the effect that, because of Eq. (48a), the value of Λ as given in Eq. (56b) has to be multiplied by a factor $\frac{1}{2}\ln5=0.805$. Assumption (a), when applied to some refractory metals, tends to overestimate the sputtering yield, as follows from a comparison with experimental yield curves. We have to leave open the question of whether this discrepancy is due to inadequacy of the sublimation energy as a measure of surface binding or to non-negligible bulk binding forces. A complication arises in semiconductors, since it is known that silicon and germanium turn amorphous after doses of the order of[88] 10^{14} ions/cm^2 for bombardment at room temperature, so that both the measured sublimation energy (3.82 eV for Si and 3.82 eV for Ge) and the cohesive energy (7.83 and 7.63 eV, respectively[89]) become questionable. Empirically, by

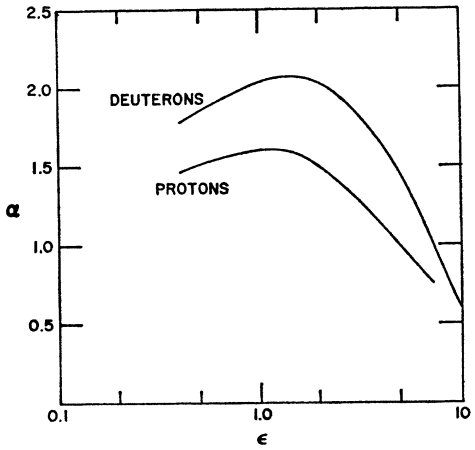

FIG. 15. Factor α in Eq. (77) for protons and deuterons incident on a heavy target, as a function of Lindhard's dimensionless energy variable (Refs. 21 and 40) $\epsilon=E[M_2/(M_1+M_2)]a/Z_1Z_2e^2$. The curves are based on Eq. (94), but should only be considered rough estimates.

[88] J. W. Mayer, L. Eriksson, S. T. Picraux, and J. A. Davies, Can. J. Phys. 46, 663 (1968).

[89] R. Bäuerlein, in *Radiation Damage in Solids*, edited by D. S. Billington (Academic Press Inc., New York, 1962), p. 358.

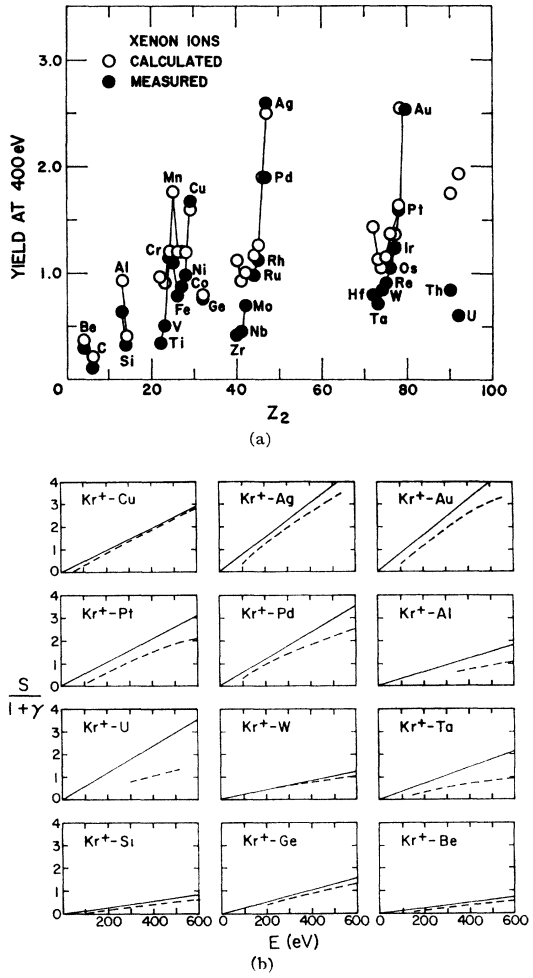

FIG. 16. Low-energy sputtering yields for Xe^+ and Kr^+ ions incident on a series of targets. Experimental results from Rosenberg and Wehner (Ref. 91) and Wehner *et al.* (Ref. 98). Theoretical results from Eq. (95). U_0 is the measured sublimation energy for metals (Refs. 70 and 92). For Si, $U_0=2E_b=7.83$ eV; for Ge, $U_0=7.63$ eV. E_b from Ref. 89 (a) Xe^+ ions of 400 eV. Not corrected for secondary electrons. (b) Kr^+ ions. Dashed curves: experimental results; solid curves: Eq. (95), corrected for secondary electrons with $\gamma=0.07$ (Ref. 1).

assuming U_0 to be given by the latter pair of values and neglecting V, one gets good agreement with experimental results, but other combinations of U_0 and V may be equally successful and more feasible. Most interesting in this connection are measurements on germanium single crystals at various bombardment temperatures[90] that clearly show that the sputtering ratio changes almost abruptly at a certain temperature. However, the fact that the yield can either decrease or increase at this temperature, depending upon crystal orientation, indicates that there is a pronounced transparency effect on the incident ion that is difficult to separate from the effect of a change in surface and bulk binding energies.

[90] G. S. Anderson, J. Appl. Phys. **38**, 1607 (1967).

i. Ion energies smaller than 1 keV. Up to the limiting energy E^*, defined in Eq. (34), we have to insert Eq. (78) for the stopping power in Eq. (77). This yields

$$S(E)=(3/4\pi^2)\alpha T_m/U_0 \qquad (95)$$

for the sputtering yield at perpendicular incidence. This expression does not depend on either λ_0 or a. Apart from the mass number M_2, U_0 is the only target property that enters Eq. (95). The quantity α is given in Fig. 13. It is well known, mostly from the experimental work of Wehner and his group (reviewed in Ref. 1), that yield curves are indeed linear at energies down to somewhat below 100 eV, especially for not-too-light ions where E^* is not too small. Figure 16(a) shows a comparison of measured and theoretical yield values at $E=400$ eV.[91–93] For xenon ions, E^* is larger than 400 eV for all targets under consideration.

The agreement is excellent with Be, Si, Cr, Ni, Cu, Ge, Ru, Rh, Pd, Ag, Ir, Pt, and Au as targets. Other targets show measured yields that are smaller by up to a factor of 2 than the calculated ones. The deviations appear systematic and are most pronounced with Ti, V, Zr, Nb, Hf, Ta, Th, and U as targets.

The variety of targets considered in Fig. 16 covers the range of mass ratios $0.069\leq M_2/M_1\leq 1.50$. In order to check the validity of the α-versus-M_2/M_1 curve for larger values of M_2/M_1, one must consider lighter ions. For Kr^+ ions, the situation turns out to be very similar as for Xe ions [Fig. 16(b)]. With Ar^+, Ne^+, and He^+ ions the comparison cannot be done in this simple way. First, the experimental data have to be corrected for secondary electron emission.[1] The correction factors are not known accurately. Second, E^* becomes so small that the yield curves are not really linear in the 100–600-eV region (see Ref. 1). Third, for He^+ ions, and to a lesser degree for Ne^+ ions, the validity of Fig. 13 is questionable, because of the assumption of an infinite medium and neglect of scattering out of the surface. Some low-energy yield curves for lighter ions will, however, be included in the curves discussed in the following section.

ii. keV heavy and medium-mass ions. For $E>E^*$, in the elastic collision region, we insert Eq. (56b) into

TABLE I. Reduced nuclear stopping cross section $s_n(\epsilon)$ for Thomas-Fermi interaction [after Lindhard *et al.* (Ref. 20)].

ϵ	$s_n(\epsilon)$	ϵ	$s_n(\epsilon)$
0.002	0.120	0.4	0.405
0.004	0.154	1.0	0.356
0.01	0.211	2.0	0.291
0.02	0.261	4.0	0.214
0.04	0.311	10	0.128
0.1	0.372	20	0.0813
0.2	0.403	40	0.0493

[91] D. Rosenberg and G. K. Wehner, J. Appl. Phys. **33**, 1842 (1962).
[92] K. A. Gschneidner, Solid State Phys. **16**, 275 (1964).
[93] P. Sigmund, Bull. Am. Phys. Soc. **13**, 1445 (1968).

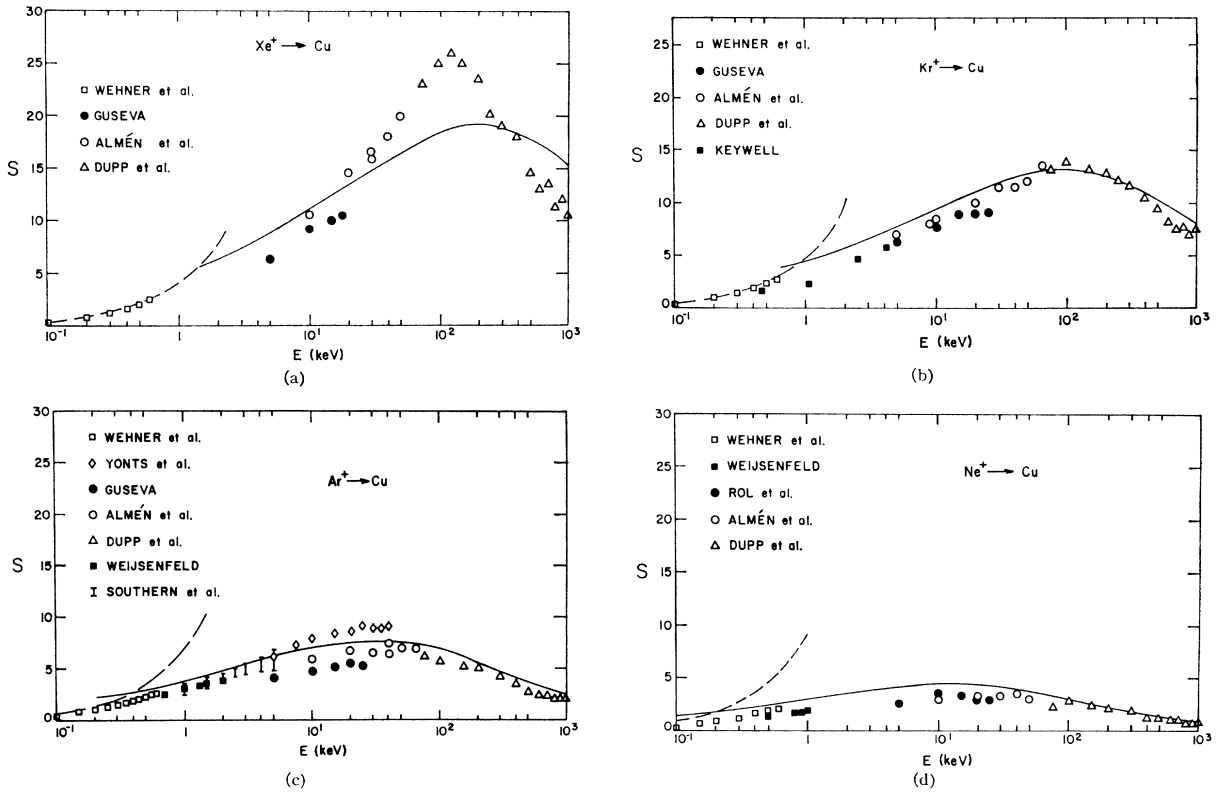

FIG. 17. Sputtering yields for Cu calculated from Eq. (97a) (solid curve) and Eq. (95) (dashed curve), compared with experimental results by Almén and Bruce (Ref. 95), Dupp and Scharmann (Ref. 96), Guseva (Ref. 97), Keywell (Ref. 5), Rol *et al.* (Ref. 84), Southern *et al.* (Ref. 80), Wehner *et al.* (Ref. 98), Weijsenfeld (Ref. 99), and Yonts *et al.* (Ref. 78). $U_0=3.51$ eV. Low-energy yields of Wehner *et al.* (Ref. 98) have *not* been corrected for secondary electrons. (a) Xe^+ ions; (b) Kr^+ ions; (c) Ar^+ ions; (d) Ne^+ ions.

Eq. (77) to obtain

$$S(E)=0.0420\alpha S_n(E)/U_0 \text{ Å}^2 \tag{96}$$

for the sputtering yield at perpendicular incidence. α is given in Fig. 13, and U_0 is the height of the surface potential. For $S_n(E)$, we take the expression of Lindhard *et al.*,[20] calculated by assuming Thomas-Fermi interaction:

$$S_n(E)=4\pi Z_1 Z_2 e^2 a_{12}[M_1/(M_1+M_2)]s_n(\epsilon), \tag{97a}$$

where

$$\epsilon=\frac{M_2E/(M_1+M_2)}{Z_1Z_2e^2/a_{12}},$$

$$a_{12}=0.8853a_0(Z_1^{2/3}+Z_2^{2/3})^{-1/2},$$

$s_n(\epsilon)$ is the universal function tabulated in Table I, and a_0 is the Bohr radius. The evaluation of Eq. (97a) for a given ion-target combination is greatly facilitated when Winterbon's tables are used.[94] One can then write

$$S(E)=0.703\frac{\alpha A_2\hat{\rho}}{\hat{\epsilon}(U_0/\text{eV})}s_n(\epsilon), \tag{97b}$$

where A_2 is the atomic weight of the target, $\hat{\rho}$ the dimensionless length unit for 1 μg/cm^2 of target material, and $\hat{\epsilon}$ the value of ϵ for $E=1$ keV. $\hat{\rho}$ and $\hat{\epsilon}$ are tabulated in Ref. 94 for many ion-target combinations. Note that the numerical constants in Eqs. (97a) and (97b) are based on the choice of $\lambda_0=24$, $a=0.219$ Å [Eq. (28′)]. Other parameters could easily be inserted by going back to Eq. (56b).

Figure 17 shows sputtering yields of polycrystalline copper for inert gas ions at perpendicular incidence, over an energy range of four decades. Mass ratios range from about 0.5 to 3. The agreement with experimental results is very good in general.[95–99] This confirms that the variation of the yield with ion energy follows approximately the Lindhard stopping power, in agreement with the conclusion of Brandt and Laubert.[10] Furthermore, the agreement is about as good at keV energies as in the eV range. This indicates that the

[91] K. B. Winterbon, Chalk River Report, No. AECL-3194, 1968 (unpublished).

[95] O. Almén and G. Bruce, Nucl. Instr. Methods **11**, 257 (1961).
[96] G. Dupp and A. Scharmann, Z. Physik **192**, 284 (1966).
[97] M. I. Guseva, Fiz. Tverd. Tela **1**, 1540 (1959); [English transl.: Soviet Phys.—Solid State **1**, 1410 (1960)].
[98] G. K. Wehner, R. V. Stuart, and D. Rosenberg, General Mills Annual Report of Sputtering Yields Report No. 2243, 1961 (unpublished), referred to in Ref. 1.
[99] C. H. Weijsenfeld, thesis, University of Utrecht, 1966 (unpublished).

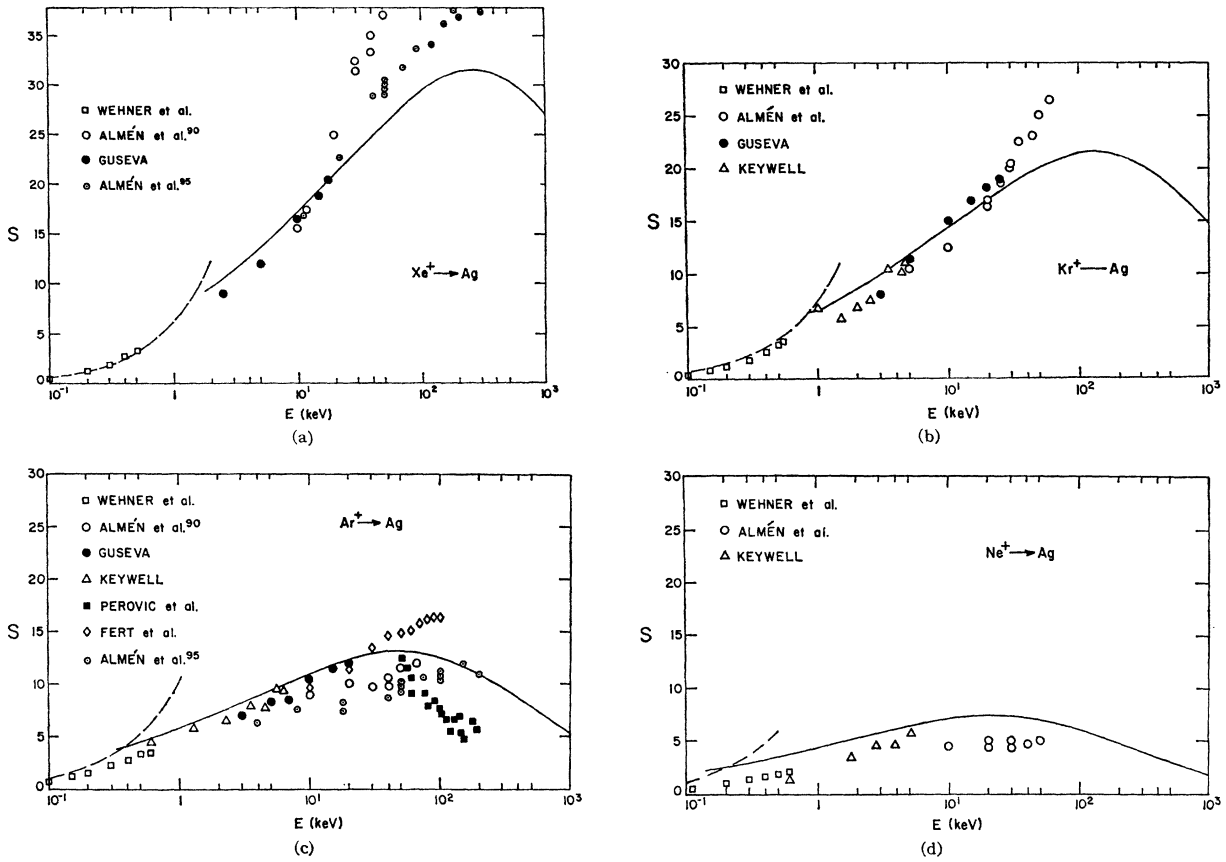

FIG. 18. Sputtering yields for Ag calculated from Eq. (97a) (solid curve) and Eq. (95) (dashed curve), compared with experimental results by Almén *et al.* (Refs. 95 and 100), Fert *et al.* (Ref. 101), Guseva (Ref. 97), Keywell (Ref. 5), Perović and Cobić (Ref. 102), and Wehner *et al.* (Ref. 98). $U_0=2.96$ eV. Low-energy yields of Wehner *et al.* (Ref. 98) have *not* been corrected for secondary electrons. (a) Xe^+ ions; (b) Kr^+ ions; (c) Ar^+ ions; (d) Ne^+ ions.

numerical value of $C_0=\frac{1}{2}\pi\lambda_0 a^2$ that did not enter the low-energy yield formula is accurate enough, at least for copper as a target. All curves extend somewhat into the inelastic collision region. The influence of electronic stopping is assumed to be small in these cases, and the good agreement at high ion energies confirms this. For neon, the sputtering yield is overestimated slightly, probably because of the neglect of the surface. The position of the maximum is not well predicted in the Xe^+-Cu curve. Although such an effect could, in principle, be caused by electronic stopping, this is unlikely for the present ion-target combination. More likely we deal with a systematic deviation of the actual stopping power from the Thomas-Fermi value. Similar effects are observed with other very heavy ions and other targets. An explanation on the basis of possible texture of the target can therefore be ruled out.

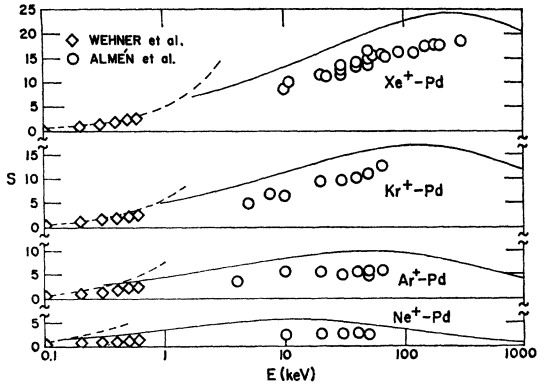

FIG. 19. Sputtering yields for Pd calculated from Eq. (97a) (solid curve) and Eq. (95) (dashed curve), compared with experimental results of Almén *et al.* (Refs. 95 and 100) and Wehner *et al.* (Ref. 98). Low-energy yields have *not* been corrected for secondary electrons. $U_0=3.90$ eV.

Figure 18 shows a similar set of yield curves for silver. The agreement between the experimental data of several groups is not as good as in the case of copper.[100–102] In the case of Almén's data,[95,100] the discrep-

[100] O. Almén and co-workers (unpublished).

[101] C. Fert, N. Colombié, and B. Fagot, in *Ionic Bombardment, Theory and Applications* (Gordon and Breach, Science Publishers, Inc., 1964), p. 92.

[102] B. Perović and B. Cobić, in *Proceedings of the Fifth International Conference on Ionization Phenomena in Gases, Munich, 1961* (North-Holland Publishing Co., Amsterdam, 1962), p. 1165.

ancy presumably stems from the texture of two different polycrystals. Unfortunately, none of the data extends to energies beyond the maximum. While the theoretical curves tend to underestimate the sputtering yield slightly (except for neon), the reverse is true in the case of palladium (Fig. 19), a metal that is very similar to silver. The discrepancy appears to be definite, and gives an indication of the accuracy of the yield formula when applied to predict absolute sputtering yields.

Figure 20(a) shows the Ar^+-Au sputtering yield, which is similar to those of copper and silver.[103] Figure 20(b) presents yields for cadmium and zinc. These metals have particularly small sublimation energies and correspondingly high yield values. The agreement with theory is surprisingly good.

All the targets discussed so far were polycrystalline. Yield measurements on truly amorphous targets have been done by Nghi and Kelly.[104] The results show that the sputtering yields of amorphous oxides do not differ substantially from those of the corresponding metal polycrystals. In some cases, amorphous yields may

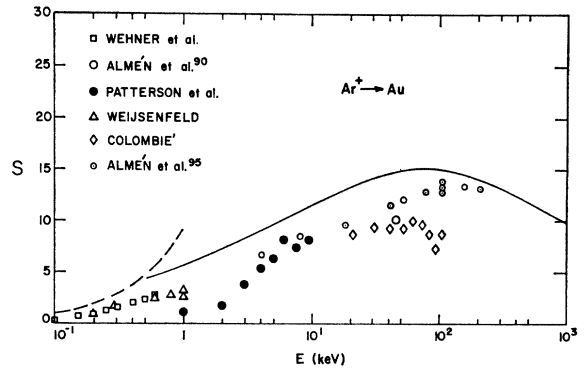

FIG. 20. Sputtering yields for argon ions. (a) Gold: Almén *et al.* (Refs. 95 and 100), Patterson and Tomlin (Ref. 103), Wehner *et al.* (Ref. 98) (uncorrected); Weijsenfeld (Ref. 99), and Colombié (Ref. 85). $U_0=3.80$ eV. (b) Zinc and cadmium: Colombié (Ref. 85). $U_0=1.36$ eV (Zn), 1.16 eV (Cd).

[103] H. Patterson and D. H. Tomlin, Proc. Roy. Soc. (London) A265, 474 (1962).

[104] L. Q. Nghi and R. Kelly (to be published).

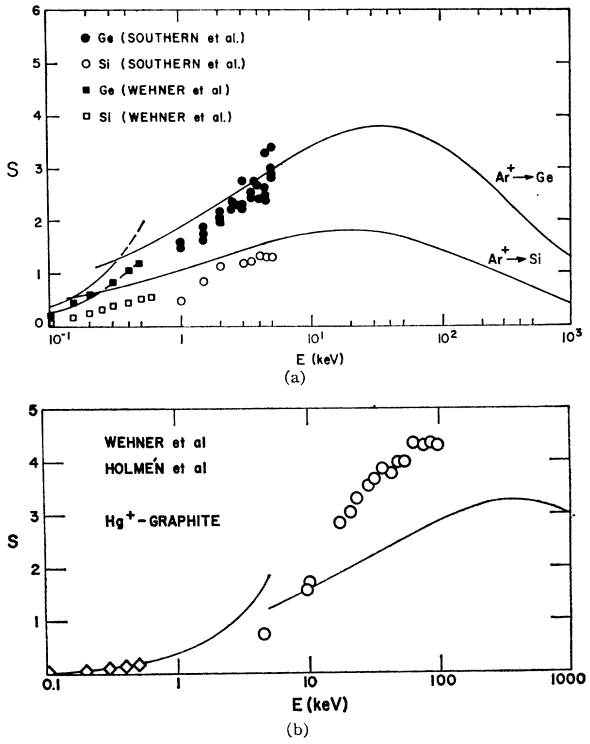

FIG. 21. Sputtering yields for "amorphous" targets. (a) Argon ons on silicon and germanium: Southern *et al.* (Ref. 80) and Wehner *et al.* (Ref. 98) (uncorrected). $U_0=7.83$ eV (Si), 7.63 eV (Ge). (b) Mercury ions on graphite: Holmén and Almén (Ref. 87) and Wehner *et al.* (Ref. 98) (uncorrected). $U_0=7.36$ eV.

even be higher. A quantitative comparison with the present theory is not possible, since the theory only applies to monatomic targets. Similar conclusions can be drawn from yield measurements on metal carbides by Gurmin *et al.*[105] Experiments on liquid targets would be of interest. Existing data[106] only deal with sputtered *ions*.

Some crystalline targets turn amorphous under ion bombardment at the doses required in sputtering experiments. Figures 21(a) and 21(b) show yield curves for Ar^+-Si, Ar^+-Ge, and Hg^+-C (graphite). In case of germanium, the agreement with theory is about as good as in copper. Silicon shows some discrepancy both at low and higher ion energies. The Hg^+-C yield curve underestimates the yield in the 10–100-keV range, but the same was true for the Xe^+-Cu and Xe^+-Ag curves. Although there are not enough data available on sputtering of monatomic amorphous targets, the observations are consistent with the assumption that our yield formula applies equally well to polycrystalline and amorphous targets.

Finally, we mention that the yield formula over-

[105] B. M. Gurmin, T. P. Martynenko, and Yu. A. Ryzhov, Fiz. Tverd. Tela **10**, 411 (1967) [English transl.: Soviet Phys.—Solid State **10**, 324 (1968)].

[106] H. L. Garvin, National Aeronautics and Space Administration Report No. NASA CR-54678, 1968 (unpublished).

estimates, in general, the sputtering yields of refractory metals, as compared with experimental results of Colombié,[85] Wehner and Rosenberg,[107] and Almén and Bruce.[95] Dependent on the ion type, these discrepancies are equally well observed at low ion energies (Fig. 16). We therefore conclude that the main reason for the discrepancy is to be found in the assumptions concerning the surface and bulk binding forces.

Not many yield measurements have been done on ionic crystals. Navinsek[108] reports yield values for Ar^+ ions on NaCl and KCl crystals. With a cohesive energy of[109] $U_0=7.50$ eV, NaCl has practically the same input parameters as silicon for the sputtering-yield formula, except that we multiply Eqs. (95) and (96) by a factor of 0.805, treating an ionic crystal as a covalent one. The predicted sputtering yields are somewhat larger than Navinsek's reported values. The difference is probably due to crystal-lattice effects, since the crystal was bombarded parallel to a (100) direction.

By comparing Fig. 17(d) with Fig. 17(a), one recognizes that the Xe^+-Cu sputtering yield is larger than the Ne^+-Cu yield for $E\gtrsim 500$ eV, while the opposite is true at smaller energies. This crossover between yield curves for light and heavy ions has been observed a long time ago,[1] and various explanations have been proposed.[110] In the present picture the crossover occurs as a consequence of the properties of the stopping-power function, and the accurate position is also determined by the α-versus-M_2/M_1 curve (Fig. 13). Since the latter is not too accurate for $M_1 \ll M_2$, the predicted values for the crossover do not always agree with the measured ones.

iii. Light ions. Experimental sputtering yields for light ions have been reported by Wehner *et al.*[98] (He^+ ions at eV energies), by Grønlund and Moore,[76] Gusev *et al.*,[77] and Yonts *et al.*[78] (protons, deuterons, and He^+ ions in the 10-keV region), and by Kaminsky[111] (deuterons above 100 keV). For several obvious reasons, application of the theory to sputtering by light ions in the eV region does not appear feasible. For the ~10-keV, region we can use α as given in Fig. 15, but we must remember that the curves are only qualitatively correct. Comparison with experimental results indicates that α is smaller (≈ 1) than predicted by Fig. 15. This may partially be accounted for by our neglect of the surface in the calculation. It is hoped that a more accurate treatment of this case will be possible in the near future.

Kaminsky's[111] ion energies are in the Rutherford region, so that $\alpha=\frac{1}{2}$ should apply. However, well-aligned single crystals were used in the bombardments, so that the assumption of random slowing down of the ions is not justified. It turns out that for both (100) copper and (100) silver crystals the measured sputtering yields are smaller by approximately a factor of 2 than the calculated random yields, for deuteron bombardment at 100 keV up to 1.5 MeV. This small difference indicates that there is no major effect (≤ 2) of channeling on sputtering yields for these projectiles, consistent with our conclusion in Sec. 5 C a iii that sputtering is determined by soft collisions in this case.

d. Backsputtering of Thin Foils and Depth Responsible for Sputtering

In Sec. 4 D we derived the result that the majority of the sputtered particles originate from a surface layer of thickness $\Delta x\approx 5$ Å. Obviously this does not mean that a film of thickness Δx would exhibit the same backward sputtering yield as a thick target. When a very thin film is bombarded, the collision cascades cannot develop as in an infinite medium, and therefore the backsputtering yield of such a film will, in general, be smaller than that of a semi-infinite medium. For example, for the Ar^+-Au case, we have $\alpha\approx 0.8$ for a thick target, according to Fig. 13. When a film of thickness $d=50$ Å is bombarded at an energy greater than 100 keV, the majority of the ions penetrate the film, with some energy loss and multiple scattering. Thus, the backward sputtering yield can be estimated roughly by use of Eq. (82b), which yields $\alpha\approx 0.2$ for $m=\frac{1}{2}$. This value is somewhat too small because of the total neglect of Ar^+ ions deflected within the film, but difference to the above value of $\alpha=0.8$ is large enough to show that the depth region that is responsible for sputtering *can* be quite large.

We define x_0 as the minimum thickness a target must have in order to essentially exhibit the sputtering yield of a semi-infinite target. In general, x_0 depends on ion type and energy, the angle of incidence, and, of course, the target material. Except at eV energies, x_0 will usually be larger than Δx. Therefore, x_0 is a property determined by the deposited-energy distribution function $F(x,E,\eta)$. Specifically, in the elastic collision region, within the range of validity of the power cross section (24a), we have seen that the length unit of a cascade is the quantity E^{2M}/NC [Eq. (73)], and that all lengths, including the average ion range and the average depth of deposited energy, are proportional to this quantity. Therefore, the depth x_0, irrespective of its specific definition, must be proportional to the ion range, i.e., increase with increasing energy. This result is in contrast to Onderdelinden's[15] concept of x_0 being a property of the target material independent of ion energy.

In order to obtain a rough estimate of x_0, we go back to Fig. 6. We realize that the deposited-energy functions drop down to practically zero at a certain distance x_0' from the surface. Now shift the distribution to the right, such that the dropoff coincides with the surface.

[107] G. K. Wehner and D. Rosenberg, J. Appl. Phys. **32**, 887 (1961).
[108] B. Navinsek, J. Appl. Phys. **36**, 1678 (1965).
[109] M. Tosi, Solid State Phys. **16**, 1 (1964).
[110] M. K. Sinha, J. Appl. Phys. **39**, 2150 (1968).
[111] M. Kaminsky, Phys. Rev. **126**, 1267 (1962).

We then deal with an ion that starts its motion at a depth x_0' inside the target and has a negligible sputtering yield as compared to an ion starting at the surface. Thus, the length x_0' is a rough estimate of the depth responsible for sputtering. Actually, x_0' is a lower limit for x_0, since an ion beam will have undergone multiple scattering when arriving at a depth x_0', and an ion moving at an oblique direction is a more effective sputterer. Figure 22 shows x_0' as a function of mass ratio in the elastic collision region as calculated from a Gaussian approximation to the distribution function, as well as the non-Gaussian approximation mentioned in Sec. 5 C a ii. x_0' was determined by matching a straight line to the distribution function at the surface $x=0$. From both Figs. 6 and 22, one concludes that x_0 is a sizable fraction of the total extension of the cascade, which is $\sim 2\langle x\rangle$. This may not be surprising in the case of $M_1 \ll M_2$, where the path length traveled by the ion is several times its average projected range, so that the ion is not "lost" for sputtering even when having traveled quite deeply into the crystal, but in the case of $M_1 \gg M_2$, one might have expected a smaller value of x_0. While the apparent uncertainty in x_0' is relatively large for $M_1 \gg M_2$ (Figs. 6 and 22), the error is not expected to be greater than a factor of 2. The reason for the large values of $x_0/\langle x\rangle$ is to be found in the relatively large ranges of recoiling atoms.

These considerations have an immediate consequence on single-crystal sputtering. When a crystal is bombarded along a low-indexed direction, the probability for the ion to undergo violent collisions is reduced bility for the ion to undergo violent collisions is reduced.[30] This will result in a smaller sputtering yield for both $M_1 > M_2$ and $M_1 < M_2$, for mutually different but obvious reasons. In order that a substantially smaller sputtering yield be observed, the ion must avoid violent collisions while traveling through a sizable portion of the depth region x_0. In the medium- and upper-keV region, x_0 is so large that the transparency of the lattice cannot account for this. Thus, for heavy- and medium-mass ions in the medium- and upper-keV region, the anisotropy of the sputtering yield appears to be a true channeling phenomenon, as proposed by Onderdelinden,[15,19] rather than an effect of transparency as believed earlier. The author would like to mention that he had to revise the standpoint he took at a recent discussion.[112]

For completeness, we also consider the case of ions in the Rutherford energy region. We calculate the deposited energy at a depth $x<0$ by a similar procedure as in Sec. 5 C a iii, i.e., we generalize Eq. (79):

$$F_{(1)}(x,E,1) = N\int_x^\infty dx' \int_0^{T_m} d\sigma_{(1)}(E,T)F(-x',T,\cos\varphi''). \quad (98)$$

[112] P. Sigmund, in Gordon Research Conference on Particle-Solid Interactions, Meriden, N. H., 1968 (unpublished).

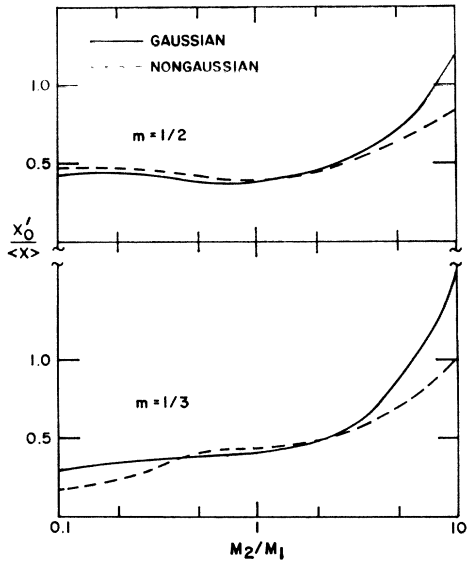

FIG. 22. Rough estimate for the ion penetration depth x_0 that is responsible for backsputtering in the elastic collision region. $\langle x\rangle$ is the average depth of deposited energy approximately of the order of the average projected range of the ion.

As in Sec. 5 C a iii, we extract the stopping power by the substitution $F_{(1)}=\alpha(x)NS_{(1)}(E)$. In case of Rutherford scattering for $d\sigma_{(1)}$, the function $\alpha(x)$ turns out to be a step function, i.e.,

$$\begin{aligned} \alpha(x) &= 0, \quad \text{for } x<0 \\ &= \tfrac{1}{2}, \quad \text{for } x=0 \\ &= 1, \quad \text{for } x>0 \end{aligned}$$

which means that x_0 is formally zero. In practice, this means that x_0 is of the order of Δx, the range of eV atoms and depth from which the sputtered atoms originate. Thus, the observed weak anisotropy of the sputtering yield of single crystals bombarded by *fast protons*[113] cannot be a channeling effect, but is to be explained by the different packing of low-indexed crystal planes and/or transparency.

This discussion of finite-depth effects had to be somewhat qualitative, since the infinite-time-and-space distributions considered in the present paper do not allow a precise determination of the relevant depths. A more detailed discussion of the anisotropy of single-crystal sputtering is being prepared for Paper III of this series.

ACKNOWLEDGMENTS

I wish to thank J. Lindhard, H. E. Schiøtt, P. V. Thomsen, K. Mika, and W. Schilling for many illuminating discussions in the early stage of this work, and T. H. Blewitt, R. M. J. Cotterill, M. S. Kaminsky, U. F. Kocks, K. L. Merkle, N. L. Peterson, and S. J.

[113] M. Kaminsky (private communication).

Rothman for their interest and encouragement during its completion. O. Almén and R. Kelly provided their recent unpublished data, and pointed out some of the numerous errors in a preliminary version of this manuscript. With D. Onderdelinde, I had an inspiring correspondence on a controversial subject. My special thanks are due to H. H. Andersen, J. A. Davies, C. Lehmann, J. B. Sanders, and K. B. Winterbon, with whom I had the opportunity to cooperate on many problems that are related to this work, and to Mrs. Vera Heitsch, who patiently and efficiently typed several editions of the paper.

PHYSICAL REVIEW VOLUME 184, NUMBER 2 10 AUGUST 1969

Deep Multistream Diffusion in Ion Implantation*

M. SPARKS
Science Center, North American Rockwell Corporation, Thousand Oaks, California 91360
(Received 6 February 1969)

Very deep penetration of ions injected into crystals has been reported in several recent experiments. These "supertails," which extend deeper into the crystals than the normal stopping range or channeling range, have the form $n_s \sim (x-x_0)^{-\eta}$, where n_s is the number of incident ions per cm^3, x is the distance from the surface of the crystal, η is typically $\sim$2–8, and x_0 is $\sim 1\ \mu$ or less. Multistream steady-state-diffusion models are developed to explain these supertails. The results agree well with published experimental data. Multistream diffusion may also be involved in other experiments, such as radiation-enhanced diffusion experiments and implantation experiments in which channeling is suppressed, but the measured concentration profiles are within the maximum channeling range.

1. INTRODUCTION

WHEN heavy ions with energies less than 1 MeV are injected into a crystal, they are stopped near the surface of the crystal, typically within a fraction of a micron.[1] But in some special cases, measurements[2–8] of the number n_S of implanted ions per cm^3 have revealed large concentrations much deeper (up to 10 μ) than the normal stopping region. All of these supertails observed to date have the form $n_S \sim (x-x_0)^{-\eta}$, with $\eta = 2$–8, where x is the distance into the crystal measured from the surface.

Although channeling[9] affords one explanation of penetration up to depths of $\sim 1\ \mu$, the supertails extending several microns deep are almost certainly not caused by channeling.[4] Previous explanations of these supertails have involved either a single-stream diffusion with a constant number of traps[4,10] or superdeep channeling.[11,12] The exponential concentration predicted by the single-stream constant-trap model could conceivably be modified by a variation in the concentration of trapping centers with distance from the sample surface, but a change of the shape of n_S from exponential to power law for four orders of magnitude change in n_S and for different samples is highly unlikely. The possibility of anomalously deep penetration due to the periodicity of the lattice has also been discussed by De Wames, Hall, and Lehman,[13] and the effect of the crystal binding of target atoms on the scattering process has been considered by De Wames and Hall.[14]

A theory is presented which explains all supertail experiments known to the author. The power-law profiles are explained by a general diffusion model, suggested by McCaldin,[15] in which several species such as vacancies, self-interstitials, and implanted ions all diffuse so rapidly that a steady state is maintained throughout the bombarding time. Kornelsen *et al.*[3] also suggested that interstitial diffusion which is stopped by vacancies might be important.

* Research performed in part at the Hughes Research Laboratories, Malibu, Calif.

[1] J. Lindhard and M. Scharff, Phys. Rev. **124**, 128 (1961). This theory, developed for gases and amorphous solids, has been supplied successfully to crystals in the normal stopping region (excluding channeling and diffusion).

[2] B. Domeij, F. Brown, J. A. Davies, G. R. Piercy, and E. V. Kornelsen, Phys. Rev. Letters **12**, 363 (1964).

[3] E. V. Kornelsen, F. Brown, J. A. Davies, B. Domeij, and G. R. Piercy, Phys. Rev. **136**, A849 (1964).

[4] J. A. Davies and P. Jespersgard, Can. J. Phys. **44**, 1631 (1966).

[5] J. A. Davies, L. Eriksson, and J. L. Whitton, Can. J. Phys. **46**, 573 (1968).

[6] H. Herrmann, H. Lutz, and R. Sizmann, Z. Naturforsch. **21A**, 365 (1966).

[7] R. W. Bower, R. Baron, J. W. Mayer, and O. J. Marsh, Appl. Phys. Letters **9**, 203 (1966).

[8] O. Meyer, Nucl. Instr. Methods **70**, 285 (1969).

[9] J. Lindhard, Kgl. Danske Videnskab. Selskab, Mat.-Fys. Medd. **34**, No. 14 (1965). See Refs. 2 and 4 for convincing channeling experiments and for references to previous channeling literature.

[10] J. O. McCaldin, *Progress in Solid State Chemistry* (Pergamon Press Ltd., London, 1965), Vol. 2, p. 9.

[11] C. Erginsoy, Phys. Rev. Letters **12**, 366 (1964).

[12] J. O. McCaldin and J. A. Brinkman, Phys. Letters **17**, 221 (1965).

[13] R. E. De Wames, W. F. Hall, and G. W. Lehman, Phys. Rev. **148**, 181 (1966).

[14] R. E. De Wames and W. F. Hall, Phys. Rev. Letters **17**, 125 (1966).

[15] J. O. McCaldin (private communication).